New Journal and we have not received input yet 31 (2022) 101280

Contents lists available at ScienceDirect

Thermal Science and Engineering Progress

journal homepage: www.sciencedirect.com/journal/thermal-science-and-engineering-progress

Mitigating the effects of partial shading on PV system's performance through PV array reconfiguration: A review

Khaled Osmani [a], Ahmad Haddad [b,c], Hadi Jaber [d], Thierry Lemenand [a], Bruno Castanier [a], Mohamad Ramadan [b,c,*]

[a] LARIS EA 7315, Polytech Angers, UNIV Angers, France
[b] School of Engineering, International University of Beirut BIU, Beirut, Lebanon
[c] School of Engineering, Lebanese International University LIU, Bekaa, Lebanon
[d] Mechanical Engineering Department, Abu Dhabi University, United Arab Emirates

ARTICLE INFO

Keywords:
Physical
Electrical
Shading
Reconfiguration
Patterns
Dispersion

ABSTRACT

This paper aims at exploring different PhotoVoltaic (PV) array Reconfiguration (PVR) methods, used to reduce the negative impacts of Partial Shading Conditions (PSCs), that could affect the performance of a PV system (i.e. hotspots, electrical mismatch, etc.). The classification of different PVR techniques is formed under three main categories: physical, electrical, and physical-electrical combination. Physical PVR alters the actual locations of the panels within the array. Referred to as static reconfiguration methods, this set includes puzzle based, number based, symmetry based, distance maximizing based, and nature inspired methods. On the other hand, electrical PVR reorders the electrical interconnections between PV panels, and is composed of algorithm based, artificial intelligence based, hybrid, and basic/improved electrical configurations. A combined PVR method hybridizes the two precedent categories. Each method from the three main sets, is critically compared to the relevant others, according to a mathematical model, which includes many performance indices: Fill Factor (FF), Mismatch Power Loss (P_{ML}), Percentage Power Loss (%P_{Loss}), Performance Ratio (PR), Execution Ratio (ER), Efficiency (η), Percentage of Power Enhancement (%PE) and DC output power (P_{DC}). The thorough investigation of different PVR techniques, resulted that a Total Cross Tied (TCT) configured PV panels, physically relocated by means of Static Shade Dispersion Physical Array Relocation (SD-PAR) algorithm, while interfered with a switching matrix controlled by Modified Harris Hawks Optimizer (MHHO) algorithm, could be an optimum and effective solution to passively mitigate PSCs' effects.

Introduction

In compliance with immense modern energy demands, a substantial need for a cheaper and reliable energy supply is globally evolving [1]. On the other hand, intercontinental collaborative projects have been established in order to reduce the effects of climate change provoked by greenhouse gas emissions, by considering renewable energy generation [2]. Among different forms of renewable energy resources, solar energy, correlated with PV systems, is a great option, due to its abundancy and the non-detrimental nature of such systems [3]. In terms of achieving the sustainable development goals, solar energy is found one of the most efficient solutions [4]. Solar power hence possesses many derived field applications to produce an environment-friendly energy, such as the utilization of solar chimney power plants [5]. A PV based energy supply possesses a high power generation capability with a zero-noise and an emission-less performance, as well as a great flexibility for an efficient usage in many applications [6].

In terms of reliability, PV systems can be integrated with thermal collectors, to produce a hybrid solar photovoltaic-thermal system, yielding in better electrical power output as well as a facility to supply hot water demands for households [7]. For instance, the energy efficiency of buildings is improved, by using photovoltaic and thermal collectors [8]: thermal panels absorb the heat from PV panels what is regarded as a bonus cooling technique [9], thus lowering the operating temperature of PV panels [10] by utilizing the waste heat of the panels [11]. The cooling effect on PV panels in turn, results in better electrical power productivity, and more energy distribution to buildings [12]. The incorporation of different types of solar panels, such as PV, thermal collectors, and concentrating solar panels, offers a combined heat-

* Corresponding author.
E-mail address: mohamad.ramadan@liu.edu.lb (M. Ramadan).

https://doi.org/10.1016/j.tsep.2022.101280
Received 3 December 2021; Received in revised form 16 March 2022; Accepted 16 March 2022
Available online 19 March 2022
2451-9049/

Nomenclature

AAR	Adaptive Array Reconfiguration
ACMS	Ancient Chinese Magic Square
AR	Automatic Reconfiguration
ARS	Automatic Reconfiguration System
ASP	Arithmetic Sequence Pattern
BCC	Bidirectional Cuk Converter
BL	Bridge Linked
BOA	Butterfly Optimization Algorithm
BPD	Bypass Diode
CS	Competence Square
D	Diagonal
DAS	Data Acquisition System
DDM	Double Diode Model
DPP	Differential Power Processing
DS	Dominance Square
DSP	Digital Signal Processor
EAR	Electrical Array Reconfiguration
ER	Execution Ratio
FF	Fill Factor
FPGA	Field Programmable Gate Array
FRA	Flow Regime Algorithm
FRPVA	Full Reconfigurable PV Array
FS	FutoShiki
GA	Genetic Algorithm
GMPP	Global Maximum Power Point
GMPPTs	Global Maximum Power Point Trackers
GOA	Grasshopper Optimization Algorithm
HC	Honey Comb
HHO	Harris Hawks Optimizer
HRPVA	Half Reconfigurable PV Array
HSV	Hue Saturation Value
IE	Irradiance Equalization
IGBT	Insulated Gate Bipolar Transistor
IMI	Irradiance Mismatch Index
IPT	Image Processing Technique
IS	Information System
KCL	Kirchoff's Current Law
KK	KenKen
KVL	Kirchoff's Voltage Law
LMPPs	Local Maximum Power Points
LN	Long Narrow
LP	Linear Programming
LS	Latin Square
LW	Long Wide
MAA	Munkres' Assignment Algorithm
MHHO	Modified Harris Hawks Optimizer
MIQP	Mixed Integer Quadratic Programming
MPP	Maximum Power Point
MPPTs	Maximum Power Point Trackers
$\%P_{Loss}$	Percentage power loss
$\%PE$	Percentage power enhancement
$[u_i]$	Equivalent class for index i
$[u_j]$	Equivalent class for index j
C_{ij}	Cell in ith row and jth column
E_0	Random variable
E_{act}	Actual produced energy
E_e	Error of currents summation
G_{F_0}	Irradiance on non-shaded submodule
G_{F_i}	Irradiance on each submodule
$GMPP_{CS}$	Case specified global power peak
$GMPP_{PSC}$	Global maximum peak at PSC
$GMPP_{STC}$	Global maximum peak at STC
$GMPP_{conv}$	Conventional global power peak
G_O	Irradiance at STCs
G_{ij}	Irradiance received by the module at the ith row and jth column
$I_{M_{ij}}$	Generated current at STCs
I_0	Diode saturation current
I_D	Diode current
I_M	Maximum output current
I_{MP}	Maximum peak current
I_{Ph}	Light generated current
I_{PV}	Cell current
I_{SC}	Short circuit current
I_{SH}	Shunt branch current
I_{Si}	String current at the ith row
I_{ij}	Module current
I_k	The current at k^{th} row of the array
K_{IJ}	Irradiance factor
K_i	Current temperature
M_{ij}	PV module at ith row and jth column
N_{P_A}	Number of parallel strings
N_{S_A}	Number of series panels in a string
N_p	Number of modules connected in parallel
N_s	Number of modules connected in series
$P_{GMPP_{PSC}}$	Maximum power at PSC
$P_{MAX_{unshaded}}$	Maximum power without any shading pattern
P_{DC}	DC Power
P_{GMPP}	Global maximum peak power
P_{Loss}	Power Losses
P_{ML}	Power Mismatch Losses
P_{PSC}	Maximum generated power at PSC
P_{STC}	Maximum generated power at STC
PV_{rated}	Rated output power
P_a	PV panel's output voltage without bypass diodes
P_{in}	Input power
P_k	The maximum output power for each code of shadow
R_{SH}	Parallel resistance
R_S	Series resistance
T_0	Temperature at STCs
T_{max}	Maximum number of iterations
α	Diode ideality factor
MS	Magic Square
MS-EC	Magic Square – Enhanced Configuration
NS	Non Symmetrical
NSCs	Non Shaded Cells
O-E	Odd-Even
O-E-P	Odd-Even-Prime
O-SDK	Optimized SuDoKu
PBA	Population Based Algorithms
P-CI	Parity-Column Index
PCM	Phase Change Material
PE	Power Enhancement
P-EC	Physical-Electrical Combined
PGI	Power Generation Index
PR	Performance Ratio
PSCs	Partial Shading Conditions
PV	Photo Voltaic
P-V	Power-Voltage
PVR	PV Reconfiguration
R	Random
RBFA	Rule Based Fuzzy Approach
RBL-HC	Rearranged Bridge Linked – Honey Comb
RBL-TCT	Rearranged Bridge Linked – Total Cross Tied
RCI	Row/Column Index
ROA	Rao Optimization Algorithm

RSP-TCT	Rearranged Series Parallel – Total Cross Tied
RST	Rough Set Theory
RTCT	Rearranged Total Cross Tied
SCs	Shaded Cells
SDK	SuDoKu
SDM	Single Diode Model
SDP	Static Shade Dispersion Positioning
SD-PAR	Static Shade Dispersion Physical Array Relocation
SIR	Sum of Irradiance
SM	Switching Matrix
SMOA	Social Mimic Optimization Algorithm
SN	Short Narrow
SP	Series Parallel
SPBC	Series Parallel with Binary Coding
SS	Sky Scraper
STCs	Standard Test Conditions
STF	Search Type Factor
SW	Short Wide
TCT	Total Cross Tied
TDM	Triple Diode Model
UC	Uneven Column
UI	Uniform Irradiance
UR	Uneven Row
ZZ	ZigZag

Symbols

$U_{rand_j}(t)$	Randomly selected position j for hawks from the population at iteration t
$U_{rand_k}(t)$	Randomly selected position k for hawks from the population at iteration t
$U_{rand_l}(t)$	Randomly selected position l for hawks from the population at iteration t
U_m	The mean position
U_{prey}	The position of the prey
V_M	Maximum output voltage
V_{MP}	Maximum peak voltage
V_{OC}	Open circuit voltage
V_T	Thermal voltage
V_k	The voltage at k^{th} row of the array
$Z_{i_{nt}}$	Solution vector of the i^{th} particle at iteration n_t
Z_i	Particle with number i
Z_j	Particle with number j
Z_k	Particle with number k
f_i	The fragrance of the i^{th} butterfly
$g^*_{n_t}$	Global best solution
g^*	Current best global solution
l^*_{nt}	Worst solution at n_t
n_t	Present iteration number
t_i	Current iteration
w_e	The weighting factor of E_e
w_f	The weighting factor of P_a
x^t_i	The i^{th} butterfly in iteration t
x^t_j	The j^{th} butterfly from the search space
x^t_k	The k^{th} butterfly from the search space
y_{iq}	Existence variable
C	Conditions set
A	Attributes set
CF	Capacity Factor
D	Decision set
E	Escape energy of the rabbit
EA	Total generated energy
ER	Execution Ratio
FF	Fill Factor
G	Actual irradiance
I	Stimulus intensity
M	Magic constant
P	Output DC power
PR	Performance Ratio
R	Relation rule
T	Actual system's temperature
U	Universe set
$U(t_i)$	Location vector in iteration t_i
V	Single diode model output voltage
a	Power exponent
c	Sensory fragrance
k	Boltzmann constant
n	Number of modules within the array
q	Electron charge
r	Random number

Greek letters

η	Efficiency

electricity production, resulting in better systems' efficiencies and faster return on investment [13].

However, a single PV module is incapable of generating a significant consumable power quantity, hence the need for interconnecting between many modules to meet higher load demands [14]. Inaccurate interconnections between PV modules, could decrease the life expectancy of the PV array, where the performance and cost efficiency of the system get diminished [15].

From the same perspective, the output of such systems is mainly dependent on radiation, environmental conditions, and ambient temperature [16]. As solar irradiance is irregularly available [17], and weather conditions are unpredictable [18], such etiologies manipulate the efficiency of a solar system, by affecting the values of series and parallel resistances (R_S and R_{SH} respectively) of the Single Diode Model (SDM) of solar cells [19]. This resultant dynamical change within inbuilt resistances becomes a challenge to be faced with [20].

Generally, irradiance conditions are subject to two distinct scenarios: either homogeneous (uniform) or non-homogeneous (partial shading). A uniform distribution of sunrays over the entire PV array, results in a single peak in the P-V (Power-Voltage) characteristic curve. On the other hand, the Partial Shading Conditions (PSCs) are met, when solar radiations are blocked by buildings, trees, poles, dust accumulation, passage of clouds and different forms of physical light obstacles. Also, shading can occur due to PV cell cracking and ageing [21]. In this case, many local peaks appear in the P-V curve [22]. There are also non-climatic triggers for PSCs, such as non-computational manufacturing designs, bad soldering bonds, and entropy of PV modules [23]. Under most circumstances, PSCs are unavoidable, due to space limitations and shadowing of adjacent PV modules [24].

PSCs have hazardous implications on the PV system's components (modules, array, etc.) and on its performance as well. For instance, hotspots are created when a portion of the PV module receives less irradiance than the unshaded portion of the same module [25]. Similarly, excessive thermal stresses play a significant role in the process of hotspots formation [26]. Shaded PV cells behave as a load while draining current from non-shaded cells, what elevates their temperature [7], and cause futuristic burnout scenes within the PV system.

PV modules are damaged due to hotspots creation, with inability to collect maximum available energy [27]. Shaded PV cells may operate in the negative voltage region causing power absorption from non-shaded cells, due to their transformation into a resistive load [28]. In other words, partial shading attenuates the PV power generation while leaving a permanent damage in PV cells [29], with a notable voltage drop on the shaded panel's terminals [30] and a reduced conversion efficiency [31]. From a different perspective, electrical mismatch for a PV array is another consequence of PSCs, where electrical differences would exist between solar cells, leading eventually to a reduction in the overall PV output power [32]. This can be noted as the power difference between faulty and non-faulty PV modules [33]. For an accurate investigation of PV output power loss, the comparison of shading pattern with the shading area is a primary factor [34]. Power output reduction in PV systems is not only proportional to the shaded area, but also dependent on different other factors, such as shade intensity and physical locations of shaded modules within the PV array [35].

As a primary solution, the usage of Bypass Diodes (BPDs), connected in shunt across each PV module, reduces the probabilities of hotspots formation by enabling a bypass route for the generated current to follow, when an open-circuit of a module is established due to shading [36].

However, the usage of bypass diodes is not an optimum solution for PSCs, due to having many limitations [37], while inducing multiple peaks in the P-V curve [38]. Aside from BPDs, Maximum Power Points Trackers (MPPTs) are considered as an effective solution for uniform shading, whereas they fail in locating a global maximum between different locals. Consequently, unbalanced PV string currents will also exist [39].

Unlike MPPTs' chase for the local maximum, GMPPTs (Global Maximum Power Point Trackers) algorithms succeed in locating the highest maximum among different locals, thus, reducing the effects of PSCs and ensuring a maximum energy harvest [40]. However, GMPPTs are regarded as costly solution, demanding extra circuitry and complex algorithms implementation (artificial intelligence, machine learning, etc.) [41].

Aside from tracking maximums in P-V curves, and in order to compress the different undesirable effects of PSCs, the micro-inverters' employment on the level of each PV module, may alleviate the energy production of the entire PV system, by mitigating the electrical mismatch issue [42]. However, this solution adds additional financial burden on the PV system's operational cost [43].

Upgraded research is moving toward PV panel reconfiguration, as a way to distribute the shading effects over the entire PV modules in the system, rather than being centered over partial fragments [44]. As a result, this helps in equalizing the produced string currents [45] after an equal shade dispersion [46]. Array Reconfiguration (AR) adjusts the P-V characteristic curve, leaving space for a single maximum peak [47]. Compared to other PSCs' mitigation techniques, AR is effective on both operational as well as economical aspects of a PV system [48]. It can be applied to compensate the effects of stationary shadows (caused by fixed objects) as well as moving shadows (caused by passage of clouds) [49].

Three major classifications are established within this paper for PV array reconfiguration strategies, as either electrical (dynamic, by means of switches/matrices), physical (static, by actual physical relocation of the PV array) [50], or the combination of the two precedents. Dynamic reconfigurations are powerful in reducing the effects of passing clouds, instantaneously. The failing events of solar modules are limited by their automatic disconnection from the array, initiated by a Switching Matrix (SM) [51]. This in turn compensates the sudden changes in irradiance profiles, sparing away the problems of reduced PV system's efficiency and lowered energy generation [52]. Due to the fact that parallel interconnections within a PV module are more resilient to shading than serially connected ones, rules are set for SM accordingly. The grouping of newly created sub-modules is based on the insulation levels of different modules [53].

On the other hand, physical reconfiguration is a single time relocation arrangement. This configuration does not change according to the instantaneous shading patterns [54], where the combinatorial techniques, utilize the characteristics of both electrical and physical configurations. In this paper, the evaluation of different techniques for PV array reconfiguration will take place, according to the stated classifications. Each general method individually contains a set of sub-methods, which will be critically compared to the corresponding others within the same set. The remainder of this paper consists as follows: Section 2 models the electrical output of a PV system, where Section 3, reveals different effects of PSCs over PV systems' performance. Section 4 represents the complete surveyed reconfiguration schemes for PV arrays, Section 5 discusses the results of investigated reconfiguration methods, where finally, conclusions and related future work are conducted in Section 6.

Electrical modelling of a PV system's output

The output of a single PV cell is too small to be considered as consumable [55]. Different serial/parallel connections are required to increase the power output of PV cells [56]. A PV module is therefore established by a number of serial/parallel connected cells [57]. PV modules in turn are allied either in parallel, series, or in series–parallel combinations to build a PV string [58]. A parallel arrangement of strings forms finally a PV array [59]. This entire process can be graphically interpreted as shown in Fig. 1.

The PV cell shown in Fig. 1 can either be emulated by a Single Diode Model (SDM), Double Diode Model (DDM) or Triple Diode Model (TDM) [60].

The procedure of extracting larger power values from PV arrays, starts from the SDM shown in Fig. 1: the output current of a PV cell is calculated after applying Kirchoff's Current Law (KCL) at node A. The resulting cell current is represented in Eq. (1) [61,62].

$$I_{PV} = I_{Ph} - I_D - I_{SH} \quad (1)$$

where I_{Ph} corresponds to the light generated current, I_D the diode current and I_{SH} the shunt branch current. To have a more precise formulation of the cell current, all of the right sided quantities in Eq. (1) must be elaborated as follows in Eq. (2), (3), and (4) [61,62].

$$I_{Ph} = \frac{G}{G_O} \bullet [I_{SC} + K_i(T - T_0)] \quad (2)$$

$$I_D = I_0 \left[exp\left(\frac{q(V + R_s I_{PV})}{\alpha kT} \right) - 1 \right] \quad (3)$$

$$I_{SH} = \frac{V + R_s I_{PV}}{R_{SH}} \quad (4)$$

with G representing the actual system's irradiance, G_O the irradiance at the Standard Test Conditions (STCs: $G_O = 1000W/m^2$), I_{SC} the short circuit current, K_i the current temperature coefficient, T the actual system's temperature, T_0 the temperature at the STCs ($T_O = 25^{\circ}C$) [63], I_0 the diode saturation current, V the single diode model output voltage, R_s the series resistance, α the diode's ideality factor, k the Boltzmann constant, q the charge of an electron, and R_{SH} the shunt resistance [61,62].

The substitution of Eqs. (2), (3), and (4) in Eq. (1), represents the expanded PV cell current shown in Eq. (5).

$$I_{PV} = \frac{G}{G_O} \bullet [I_{SC} + K_i(T - T_0)] - I_0 \left[exp\left(\frac{q(V + R_s I_{PV})}{\alpha kT} \right) - 1 \right] - \frac{V + R_s I_{PV}}{R_{SH}} \quad (5)$$

By referring to Fig. 1, a clear formulation for the PV module current, can be achieved by taking into consideration the amount of irradiance striking on the correspondent module with respect to G_O. Hence, Eq. (6) represents the module current I_{ij}.

$$I_{ij} = \frac{G_{ij}}{G_O} \bullet I_{M_{ij}} \quad (6)$$

where $I_{M_{ij}}$ represents the generated current at STCs [64], by the module

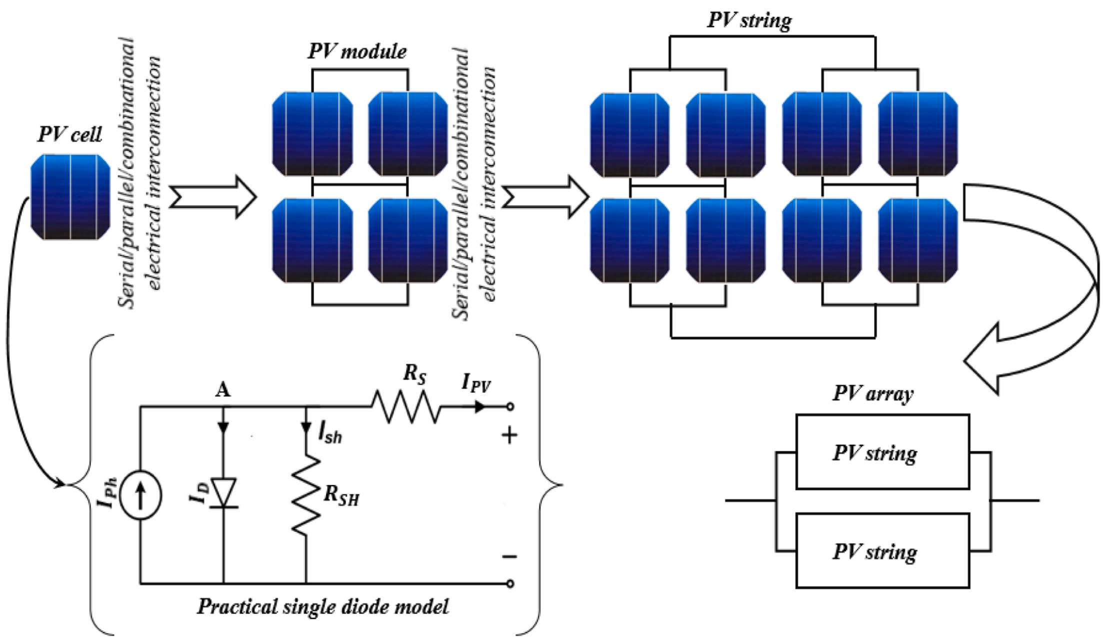

Fig. 1. The composition of a PV array from PV cells.

located at i^{th} row and j^{th} column in a PV array, with G_{ij} the irradiance received by the same module.

Additionally, the string currents depend on the PV modules' electrical interconnections, such as TCT (Total Cross Tied), SP (Serial Parallel), HC (Honey Comb) etc. However, a generic row current (delivered by a PV string) can be calculated with respect to the module's current as represented in Eq. (7), when the string is formed by successive PV modules connections in series [65].

$$I_{Si} = \sum_{i=1}^{i_{max}} K_{IJ} \bullet I_{M_{ij}} \tag{7}$$

where I_{Si} indicates the string current at i^{th} row and K_{IJ} the irradiance factor which equals to G_{ij}/G_O.

Successively, the PV array current depends on the values of resulting string currents, which in turn are dependent on how the strings are connected. For the generic case of serial/parallel electrical interconnections between different PV strings, the PV array current can be calculated according to Eq. (8) [66].

$$I_{Array} = N_p\left\{I_{Ph} - I_0\left[exp\left(\frac{V + R_sI_{PV}}{\alpha N_sV_T}\right) - 1\right]\right\} - \frac{V + R_sI_{PV}}{R_{SH}} \tag{8}$$

where N_p and N_s denote the number of modules connected in parallel and series respectively, and V_T the thermal voltage [61].

The stated current calculations are the first indicators that judge the performance of the PV system [67]. For instance, partial shading can be detected from the PV cell to PV array levels. In other words, when a PV cell gets shaded, its produced current would be much smaller than the other receiving complete solar radiations [68].

The distinction between these two currents classifies PV cells as healthy or faulty. Similar perspective can be executed on the levels of PV modules, strings, and arrays. Non-shaded PV arrays would have zero string currents differences, thereby generating more power [69]. When partial shading exists, the differences between various string currents, indicate the creation of several LMPPs (Local Maximum Power Points) and a GMPP (Global Maximum Power Point) in the characteristic P-V curve [70]. By taking this into acknowledgment, a case-specified PV array reconfiguration would ensure that the PV system is delivering the highest available power [71].

Effects of partial shading on PV system's performance

With various reasons triggering partial shading scenarios over a PV system, hazardous effects can be seen affecting its operational behavior [72] as represented in Fig. 2. In PSCs, the PV array's composers (modules, strings) receive inhomogeneous solar irradiance [73]. The PV output energy is aggravated due to the mismatch in the electrical characteristics [74]. Resultant consequences can be summed up as follows [75]:

- Hotspots
- Multiple peaks
- Electrical mismatch losses

Hotspots

When the operating current of a PV module exceeds its short circuit current I_{SC}, hotspot heating occurs [76]. Hence, shaded PV cells generate less current [77] as exposed in Fig. 3. Shaded Cells (SCs) are obliged to carry a higher current originated from Non-Shaded Cells (NSCs) [78]. Accordingly, SCs operate as a load, and consume power from NSCs. This behavior compels an elevated temperature inside the cells. Consequently, PV modules get permanently damaged [79].

Multiple peaks

When the PV array examines a reduced power output due to PSCs, after activation of bypass diodes, a new problem arises, such as the apparition of multiple peaks in the P-V characteristic curve [80], as shown in Fig. 4. This fact acts as an obstacle in front of MPPTs, where such trackers are forced to locate a global peak among many locals [81]. This, in turn, adds hardware/software complexities in MPPT's design, the fact that would be reflected as an economical burden on the PV system design.

Electrical mismatch losses

Mismatch losses in a PV module occur when SCs act upon non-standard parameters [82], with increased values of series resistance R_S

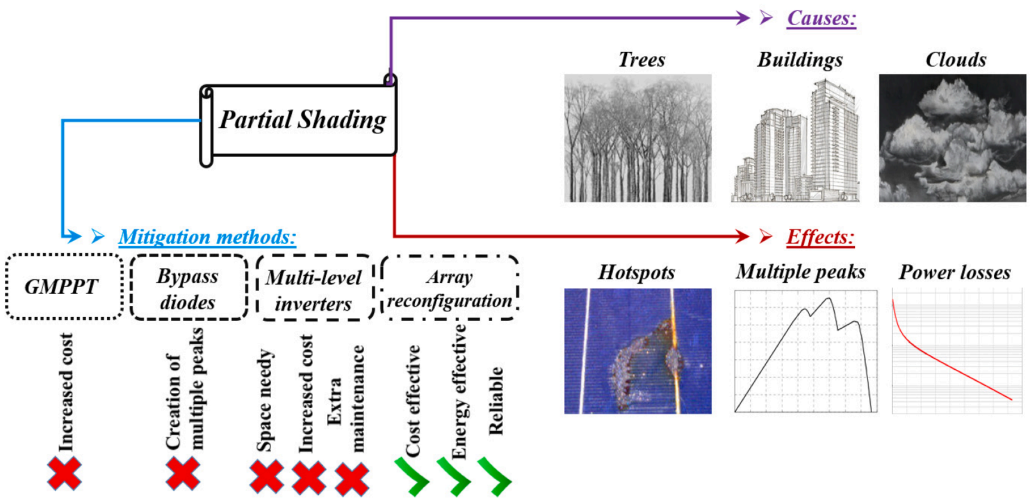

Fig. 2. Causes, effects and mitigation methods of partial shading.

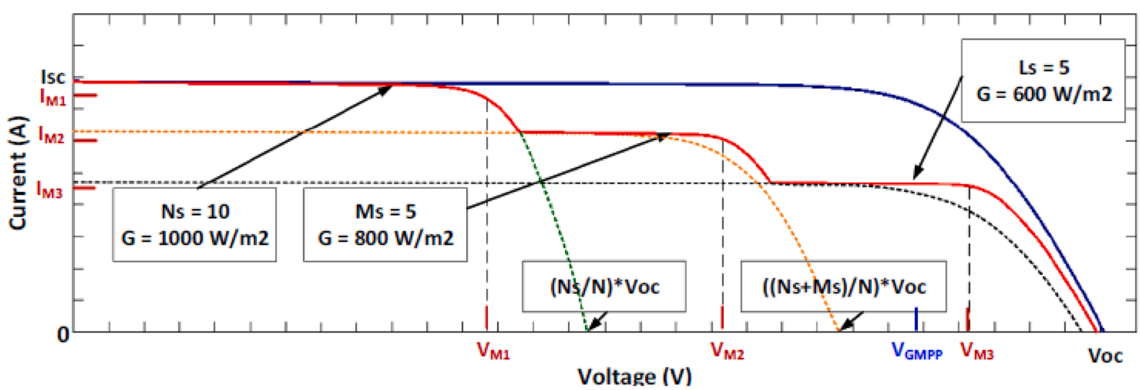

Fig. 3. Fluctuations in generated currents between shaded and non-shaded PV cells [81].

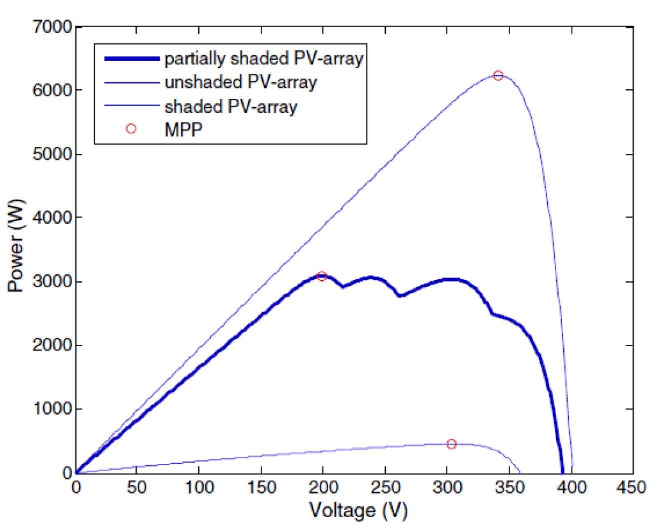

Fig. 4. Multiple peaks apparition in the P-V characteristic curve due to PSCs [78].

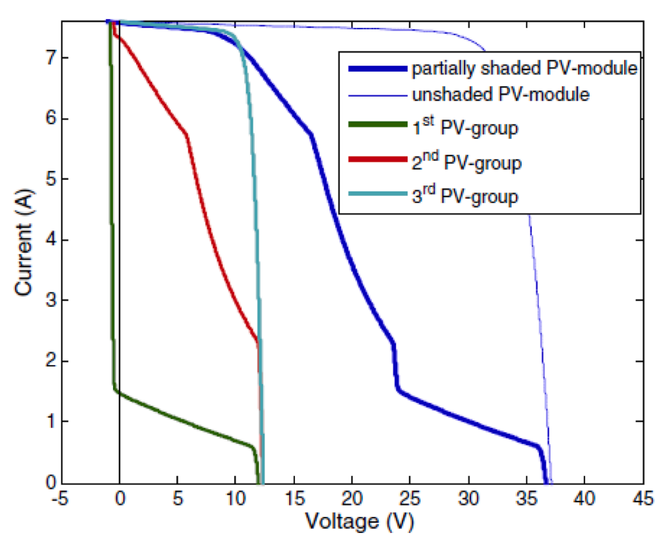

Fig. 5. Abnormalities in P-V characteristic curve due to PSCs [78].

and shunt resistance R_{SH} [83]. The resulting generated current I_{PV} becomes abnormal in both quantity and waveform [84], as indicated in Fig. 5. In other words, the output current from parallel connected blocks is hence lower than the one resulting from non-shaded blocks. A blackout can be noticed on the output power level of shaded blocks (complete open-circuit) [85].

Different negative impacts of PSCs do not depend only on the intensity of shading, but also on the shading pattern [86], as encapsulated in Table 1. Regardless of their types (hotspot, mismatch, etc.), they all share in common a heat generation ignition phenomenon on the level of PV cells, reflected as elevated operating temperatures over exceeding limits. The heat-efficiency relation of PV cells is inversely proportional, where the higher their operating temperature is, the lower the power productivity [87]. This damaging consequence affect the PV characteristic curves, by lowering the open-circuit voltage quantities, hence disturbing the overall efficiency of PV power plants [88].

Accordingly, modern research focuses on the thermal management of PV systems, as a way to mitigate the heat generation aspect produced by PSCs, such as usage of nanofluid [89], finned heat sinks based cooling [90], water based cooling systems [91], Phase Change Materials (PCM) [92], and other techniques [93].

Alternatively, and despite the effectiveness of these PV thermal regulation methods, the PVR techniques can help in mitigating excess temperatures' effects and restoring the cells' operating temperatures as nearest to STCs, with less needs of additives over the PV system's components.

Accordingly, for an effective shading dispersion from a PV array, regardless of its configuration, and PV cells raw materials used [102], an optimum PV shading mitigation predictability system must take into consideration the different patterns stated in Table 1. As a graphical interpretation, Fig. 6 lists the eight different shading patterns.

Reconfiguration schemes for PV arrays

Since PV systems are considered as lifetime investments [103], with elevated capital costs [104], the supposed payback period is averaged of 25 years [105]. During their lifecycle, a stable efficiency [106], and solid performance [107] are presumed. However, such systems often interact with unfavorable climatic conditions, such as weather fluctuations, and mainly partial shading conditions [108]. The stated problematic scenarios cannot be avoided since PV systems are of outdoor nature.

Consequently, power losses are significant due to PSCs, which would decrease the popularity of such systems, by lowering their suitability as a robust alternative power supply [109]. To overcome these drawbacks, PV reconfiguration methods can adapt the arrays to produce higher power quantities, thus increasing the overall PV systems' efficiencies [110]. Three major classification for PV Reconfiguration (PVR) methods can be addressed as [111]:

- Physical (or static)
- Electrical (or dynamic)
- Physical-Electrical Combined (P-EC)

Table 1
Different shading patterns.

Shading pattern	Description	Ref.
Uneven row shading	Happens when physical barriers shadow more rows within the array than the others	[94]
Uneven column shading	Happens when physical barriers shadow more columns within the array than the others. This can also take place when the composers (modules) of the same column are unevenly shaded	[95]
Diagonal shading	Similar to uneven row/column shading, but the physical barrier is confronted in front of the array with an inclination angle	[96]
Random shading	Does not follow any uniform shading pattern	[97]
Short and narrow shading	Caused by nearby objects, where it can be the result of adjacent PV panels shading. It covers up 25% of the total PV array space	[98]
Short and wide shading	Similar to short and narrow shading, but covers more from the total PV array space, up to 70%	[99]
Long and narrow shading	Similar to uneven row shading, but with larger shading area of 50%	[100]
Long and wide shading	Similar to long and narrow shading, but with larger shading area of 75%	[101]

Physical reconfiguration methods

Without altering the electrical connections between the PV modules, their physical locations are statically rearranged only once [112]. Based on the reconfiguration's execution on the level of PV modules, the physical reconfiguration methods help in dispersing the shade uniformly within the PV array [113]. Consequently, the mismatch loss is greatly reduced, in the same time as the power generation is increased. Table 2 encloses different classification criteria for different static PV reconfiguration methods.

Puzzle based

SuDoKu (SDK). SuDoKu is a logic-based number placement puzzle [114]. Its aim is to maintain the digits from one to nine in each block (3 × 3 sub-matrices) of the puzzle without repetition [115]. Also, each row and column should follow the same procedure by withstanding same digits under the same law [115].

When adapting a SuDoKu approach to physically rearrange PV modules, the column number remains unchanged, but the row is altered [116]. As an example in reference [117], the PV panel corresponding to the 3rd row, 3rd column is physically relocated to the 9th row, while keeping the same electrical connections as within the 3rd row. This process can be graphically interpreted in Fig. 7.

For a 9 × 9 PV array, the corresponding output voltage is denoted in Eq. (9).

$$V_a = \sum_{m=1}^{9} V_m \tag{9}$$

with V_a indicating the PV array voltage and V_m the voltage of the panel at the m^{th} row [118].

On the other hand, and for the same PV array's architecture, its current at each node can be formulated as in Eq. (10).

$$I_a = \sum_{n=1}^{9} I_{mn} - I_{(m+1)n} = 0 \tag{10}$$

with I_a as the PV array current, I_{mn} the current at m^{th} row, n^{th} column [118].

In other terms, the electrically adjacent panels, which belong to a particular row, are physically separated, and then relocated in different positions in other rows.

For a good shade dispersion, the SuDoKu method needs additional wiring, and can be only effective for a symmetrical $(m \times m)$ matrix. Consequently, this method presents high line losses (due to the extended wire lengths) with a poor dispersion factor [119]. Such drawback can be surpassed by an optimized SuDoKu physical rearranging method [120].

Optimized SuDoKu (O-SDK). Line losses seen in basic SuDoKu arrangement, are directly related to wire lengths (increased lengths signifies increased resistances) [121]. Accordingly, the Optimized SuDoKu (O-SDK) arrangement mainly focuses on shortening the interconnection wires as much as possible. The puzzle construction is established according to the following logic sequence [122]:

1. The first column of the puzzle is filled by digits from one to nine in ascending order.
2. The subsequent columns are shifted by three, concerning the maximum sub-array size from previous columns.
3. In order to avoid the arrangement of the first column in the fourth, an offset is added to the shifting process. Consequently, the second element starts from one, and the subsequent two columns are shifted by three, correspondingly to the previous column.
4. By incrementing the offset, the seventh column is filled.

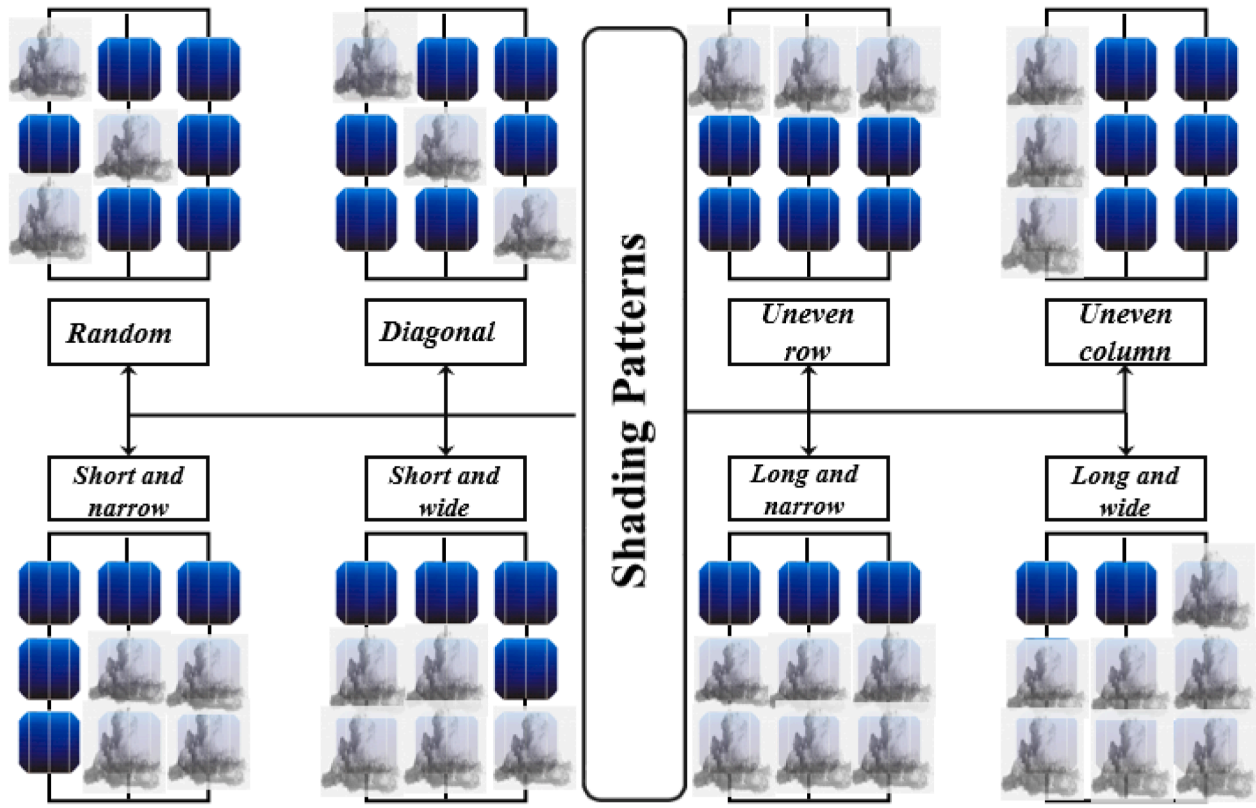

Fig. 6. Graphical representation of shading patterns.

Table 2
Major classification of physical PVR.

Physical PVR methods	Description
Puzzle based	The arrangements of PV arrays are done by mimicking the puzzle solving strategies. This set of methods include SuDoKu, optimized SuDoKu, Skyscraper, Futoshiki, Kenken and other puzzle patterns.
Number based	PV modules are arranged concerning their row/column indexes such as odd, even, etc.
Nature inspired	PV modules are arranged by imitating natural river flow behavior, which is believed to bring prosperity in life, including Lo Shu concept.
Symmetry based	Considering equal proportioning and balancing, PV modules are rearranged in a harmonious strategy, facing each other symmetrically around a defined axis.
Distance maximizing	In order to avoid mutual shading of adjacent PV modules, while taking into consideration the limited available installation area, the modules are rearranged with maximum available distances between them.
Algorithm based	The search for an optimum PV modules arrangement is conducted by means of an algorithm, including Static Dispersion Positioning algorithm, etc.

The optimized SuDoKu algorithm can be mathematically justified in Eq. (11) [122].

$$Shiftforthcolumn = \left[\frac{n-1}{3}\right] + 3 \times ((n-1)mod3) \tag{11}$$

with $\left[\frac{n-1}{3}\right]$ denoting the greatest integer function and n the correspondent column's number.

This method succeeds in eliminating the drawbacks of a conventional SuDoKu arrangement, but still have a problem in developing number repetition for non-symmetrical ($n \times m$) sub-arrays [122].

Competence square (CS). The position of a PV panel is represented by an alphabet/number representation of the form X_{mn}, where X is the alphabetical row order, m is the row's number and n the column's number. The logical flowchart of the Competence Square (CS) method can be described according to the following four rules [123]:

The a_{11} panel is randomly repositioned within the puzzle. The alphabetically successive panel is displaced according to 'L' shape.
While 'L-shaping' successive panels, if > 9, the series is resumed from next row with second column.
Following the same process, when > 9, the series is resumed from the second column with next row position.
In the last stage of puzzle construction, if an alphabet occupies a previous place, then it should be moved to the nearest forward position in the same row.

Figure 8 reveals the final positioning of PV panels according to CS method, in an 9×9 array configuration.

The proposed CS reconfiguration method has showed an effectiveness in power enhancement by a maximum of 24.4% for short and wide shade patterns, and a minimum of 6.6% for short and narrow shade patterns. From another side, CS have lowered the power loss resulting in a PV system by 49% under long and narrow shade patterns and 30% under short and narrow shade patterns [123].

SkyScraper (SS). The Skyscraper formulation is based on the height of buildings (which represent the adjacent sides of rows/columns), that can be seen through a single sight [124]. The visibility of buildings must be evaluated from four adjacent sides, what would in turn increase the method's success probability. Its flowchart operates according to the following six steps [124]:

1. Selection of $(m \times n)$ matrix size.
2. Identification of visible buildings blocks.

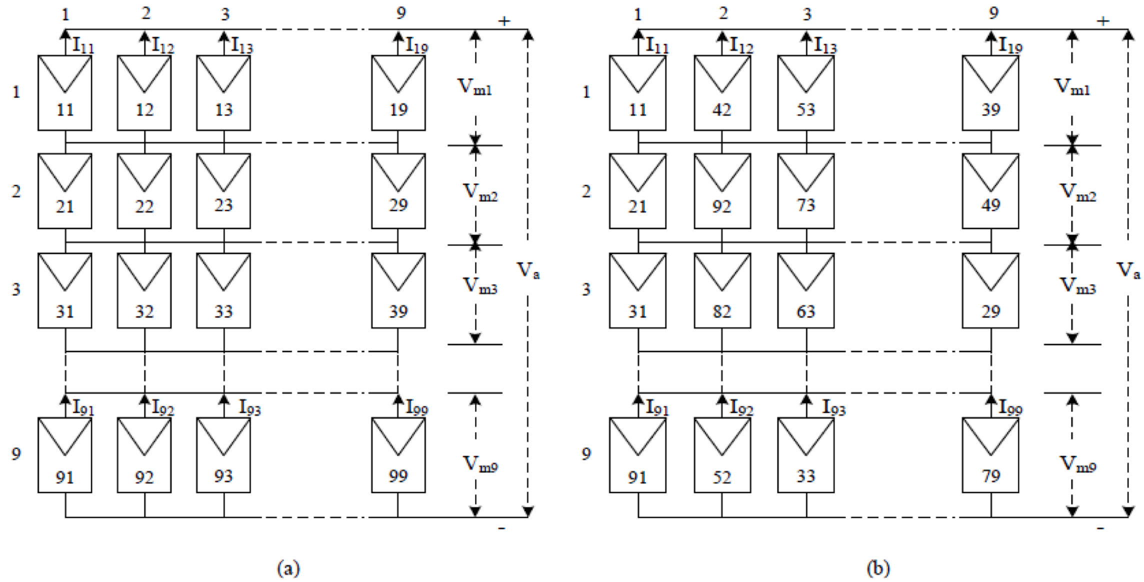

Fig. 7. PV array reconfiguration (a) before SuDoKu; (b) after SuDoKu [117].

56	66	76	86	76	16	26	36	46
37	47	57	67	77	87	97	17	27
18	28	38	48	58	68	78	88	98
89	99	19	29	39	49	59	69	79
61	71	81	91	11	21	31	41	51
42	52	62	72	82	92	12	22	32
23	33	43	53	63	73	83	93	13
94	14	24	34	44	54	64	74	84
75	85	95	15	25	35	45	55	65

Fig. 8. PV panels allocation using CS method [123].

3. Identification of total number of sub-blocks.
4. Reconfiguration of PV array based on maximum height possible in the building.
5. The PV array is another time reconfigured based on the first intermediate building height.
6. A total reconfiguration for PV array is done according to each individual sub-array reconfiguration.

The resultant final SS rearrangement is shown in Fig. 9.

The proposed physical PVR method reduces high computational burden seen in other puzzle-based reconfiguration methods (such as SuDoKu, optimized SuDoKu, etc.), with a greater dispersion factor [124].

Magic square (MS). Magic Square (MS) method is a logic based number placement puzzle, utilized to spread the shading effect, in which square grids have a special number arrangement [125]. The specialty in the number arrangement reflects in obtaining the same number after adding n digits in all rows, columns, and diagonal patterns, labelled as the magic constant M. The first number is stored at location $(n/2; n-1)$. In order to locate the succeeding number, a decrement/increment by 1 is held for

41	92	63	24	35	86	17	78	59
21	72	53	44	15	96	87	68	39
81	32	13	64	75	56	47	28	99
61	42	83	34	95	16	27	58	79
11	22	73	54	65	46	97	38	89
31	52	93	74	85	26	67	48	19
71	12	43	84	55	66	37	98	29
51	82	23	94	45	36	77	18	69
91	62	33	14	25	76	57	88	49

Fig. 9. Skyscraper PV rearrangement [124].

the previous row/column numbers respectively. If number repetition exists, the row's position is instead incremented by 1, where the column's position is decremented by 2. If the calculated row number is negative, and the calculated column position is n, the new position is held at $(0; n-2)$. This can be graphically interpreted as shown in Fig. 10 [126].

The 'n' order of a magic square is an arrangement of n^2 distinct integers, in which the rules for setting a 4×4 magic square are set according to the n^{th} element concerning the i^{th} row and j^{th} column of a pattern n_{ij} as shown in Eq. (12) [126].

$$n_{ij} where \begin{cases} i = numberofrow(i = 1, 2, \cdots) \\ j = numberofcolumn(j = 1, 2, \cdots) \end{cases} \tag{12}$$

The rules of row/column-wise additions are shown in Eqs. (13) and (14) respectively [126].

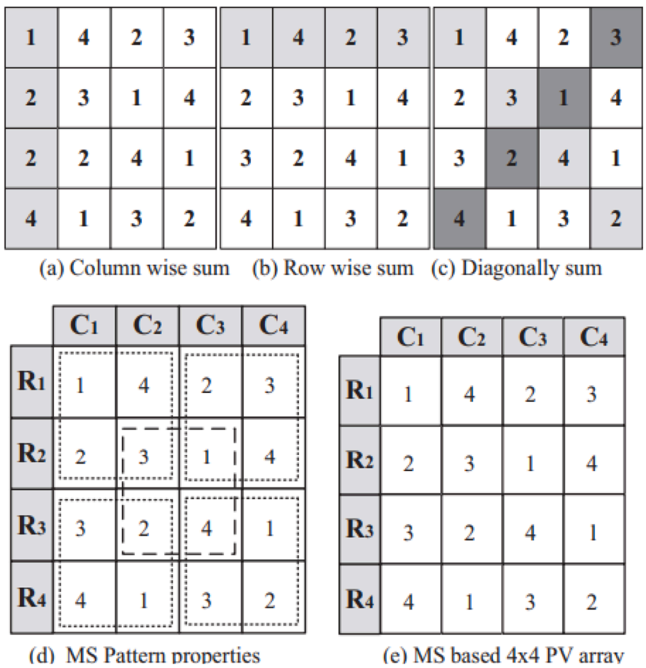

Fig. 10. Magic Square PV array arrangement [126].

$$\sum_{i=1}^{i=4} n_{ij} = MagicSumfori^{th}row(i = 1, 2, 3, 4) \quad (13)$$

$$\sum_{j=1}^{j=4} n_{ij} = MagicSumforj^{th}column(j = 1, 2, 3, 4) \quad (14)$$

The rules for diagonal-wise additions are shown in Eqs. (15) and (16) [126].

$$\sum_{j=1}^{j=4} n_{ij} = MagicSumfor(i = j) \quad (15)$$

$$\sum_{i=1}^{i=4} n_{ij} = MagicSumfor(j = i^{max} - (i - 1)) \quad (16)$$

Following the Eqs. (13) to (16) the MS configuration is obtained, where power loss is minimized, and fill factor is increased in the proposed PV system under investigation [126]. When using a GA (Genetic Algorithm) to obtain the optimal MS configuration, the maximum power output can be improved under different PSCs [127].

Dominance square (DS). The Dominance Square (DS) method has a similar approach of the CS based PV arrangement. The difference lies in the procedure while reshaping the PV panels, where instead of placing the successive modules in 'L' shape, they are diagonally rearranged. Other than that, the same four rules seen in CS method apply as well to DS method [128]. The difference can be noted when comparing Fig. 8 to the DS arrangement shown in Fig. 11.

FutoShiki (FS). The pattern arrangement is done using a Linear Programming (LP) approach in a FutoShiki (FS) based puzzle pattern [129]. The numbers from 1 to 'n' are arranged to make each row/column of a square grid, only include unique numbers, without any repetition [130]. Within the square grid, each number must obey the rule of inequality constraint between the two adjacent numbers. Ensuring a unique solution for the equidimensional square grid (i.e., FS puzzle reflected as the PV array), LP generates a proper combinatorial logic, to avoid any number repetition in each row/column. The application of the formalized logic of numbers in FS puzzle (no repetition, etc.), is translated as the equalization of the produced output power between shaded and non-shaded PV modules. The proper FS arrangement can hence modify currents/voltages quantities in each row, to homogenize the produced power, thus dispersing the shade. Fig. 12 represents the

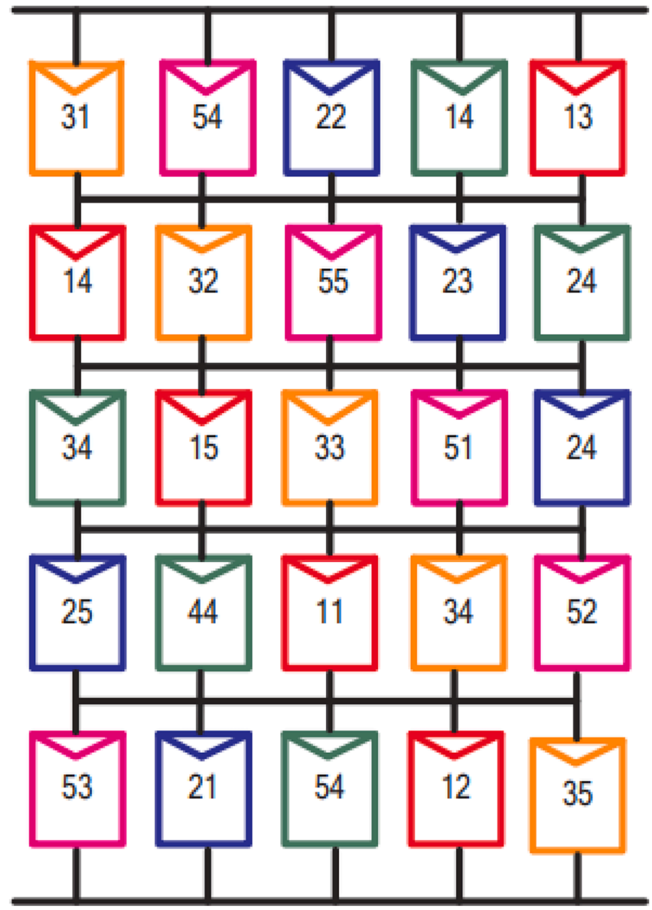

Fig. 11. Dominance square PV array reconfiguration [128].

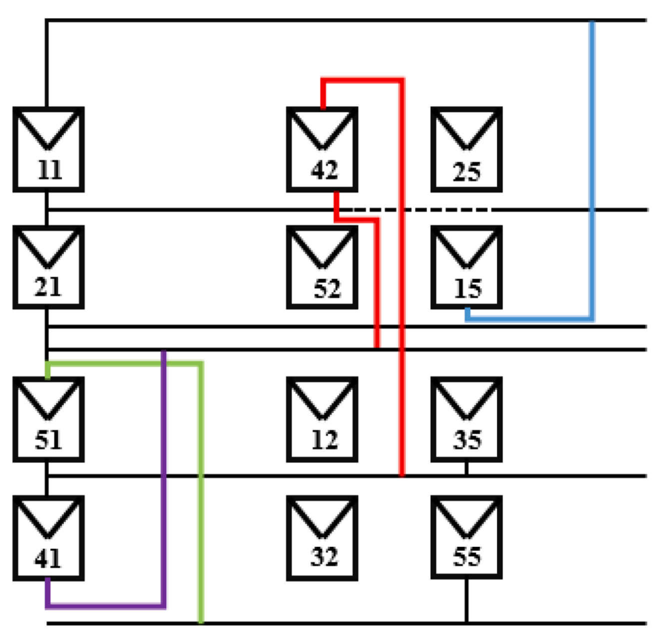

Fig. 12. Futoshiki based PV array arrangement.

Futoshiki puzzle arrangement for a PV array.

The proposed Futoshiki method disperses the shade affecting the modules in a single row, to other rows [130].

Latin square (LS). A Latin Square (LS) puzzle composes of square grids, in which the first column contains digits from one to six in ascending order [131]. Consequently, the second column's digits are shifted downward, row-wise, by 1 successively. The cell in this method is represented by C_{ij} with i, j denoting the row and column indexes respectively. The arrangement follows the basic properties shown in Eqs. ((17)-(18)) [131].

$$fori = j : \{C_{ij} = C_{(i+1)(j+1)} = C_{(i+2)(j+2)} = C_{(i+n)(j+n)}\} \tag{17}$$

$$fori \neq j$$

$$: \begin{cases} C_{ij} = C_{(i+1)(j+1)} = C_{(i+2)(j+2)} = C_{(i+n)(j+n)}, when(i+n < p, j+n < q) \\ C_{(i+n)(j+n)} = C_{(i+n-N-1)(j+n+1)}, wheni+n = p \\ C_{(i+n)(j+n)} = C_{(i+n+1)(j+n-k+1)}, whenj+n = q \end{cases} \tag{18}$$

with p, q representing the panel's row and column numbers respectively. The LSP method has a power enhancement of 6.81% compared to SuDoKu, with a reduced power loss of 13.78% [131].

KenKen square (KK). KenKen puzzle is formed by a grid surrounded by bold lines, which contains $m \times n$ square blocks. The procedure of number filling inside each block ensures the avoidance of number repetition is each row/column pattern. Each sub-grid is in turn decomposed into blocks, where according to an additive mathematical feature, the numbering (reflecting the arrangement) can be achieved [132]. Using this type of PVR, shade is dispersed across the entire PV array.

ZigZag (ZZ). By relocating the PV panels in their original columns, but in different row positions, with modules in the first row reconnected as the diagonal element, the novel ZigZag (ZZ) scheme in reference [142], can straighten the array P-V characteristics, thus decreasing the number of local maxima. Each column's elements (which represent a PV module) are kept within the same column: no horizontal shifting is made between alternate columns. From another part, rows' elements are interchanged (vertically shifted), such that the row's index of the first element is kept all along the diagonal path $(11, 12, 13, \cdots, (finalrowindex - 1)(lastcolumnindex))$. In other terms, first row's modules for instance are each shifted to the diagonal path, where the remaining modules are reconnected in row-wise manner. The ZZ strategy is flexible in applications, as it can be employed to PV arrays of any dimensions, especially for large PV farms.

AdDoKu. As an improvement for the SuDoKu method, the novel AdDoKu has achieved better results, in PV power productivity, under many PSCs. The targeted PV array consists of nine 3×3 sub-array

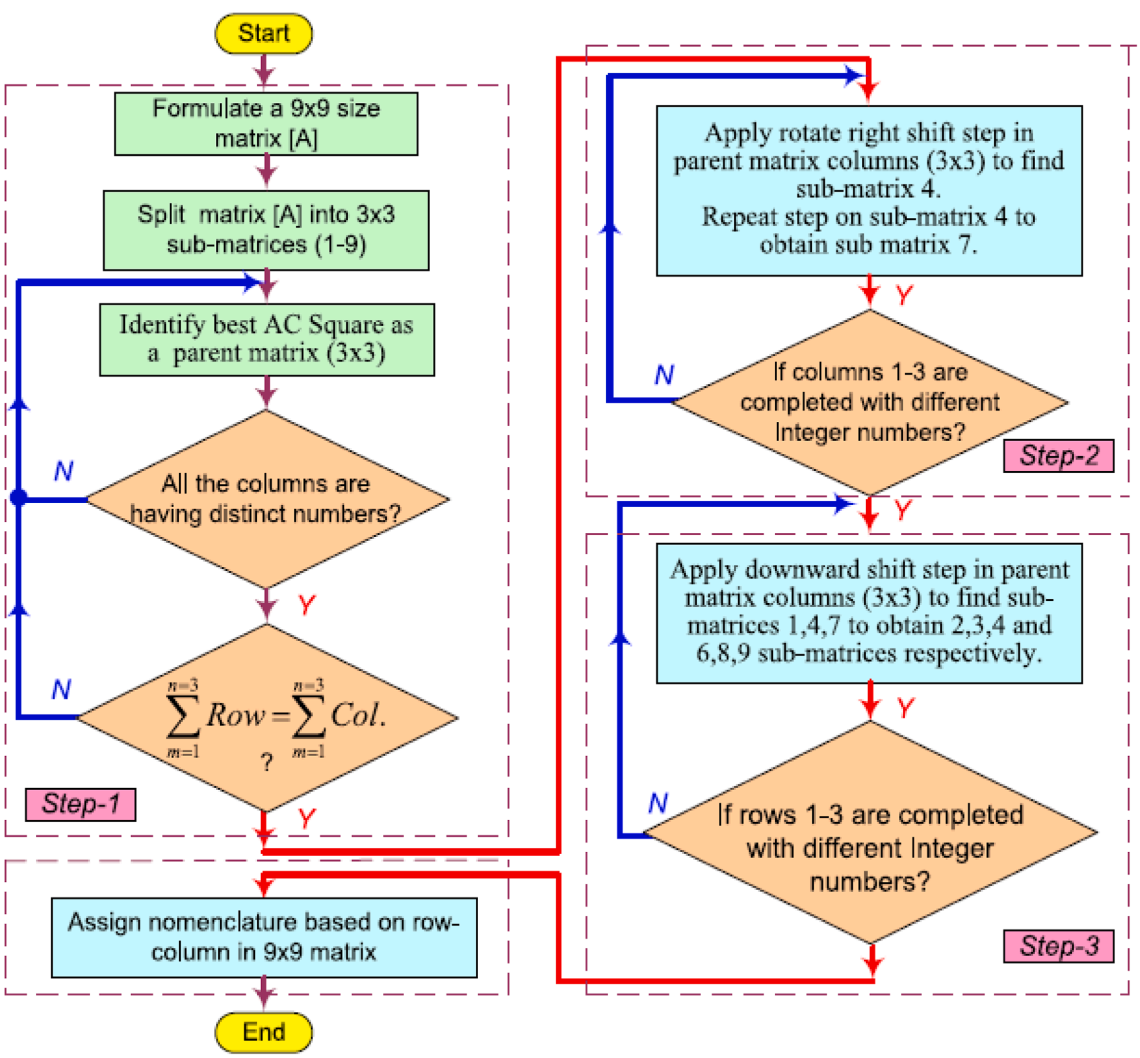

Fig. 13. The proposed ACMS based PVR method flowchart [134].

matrices, such that each row/column contains digits from 1 to 9 for only once. Each 3 × 3 sub-grid must in turn have digits from 1 to 9 only once. Eventually, the small number in the corner of a cells' group equals to the summation of the numbers in this group. Such logic based puzzle is formed using backtracking method [133]. The AdDoKu arrangement surpasses the performance of SuDoKu under all PSCs test, however it lacks experimental approval.

Ancient Chinese Magic square (ACMS). The Ancient Chinese Magic Square (ACMS) can effectively disperse shades over the entire PV array, where the parent ACM matrix is derived following the row/column/diagonal summations equality properties. As similar to SuDoKu method, to solve a 9 ×9 PV matrix, the ACMS technique's flowchart is presented in Fig. 13, with general rules as follows [134]:

i. Re-arrangements are done according to the best observed ACM matrix
ii. Columns are right shifted
iii. Rows are downward shifted

Despite the fact that ACMS have surpassed many other puzzle-based PVR methods, still its tested shading patterns conditions were narrow.

Arithmetic Sequence pattern (ASP). The Arithmetic Sequence Pattern (ASP) technique is proposed to reduce wire losses, and shading dispersion over sub-arrays, as in the case of other puzzle-based PVR methods, such as SuDoKu, FS, MS, etc. The reconfigured modules arrangements do not imply any radical change in the initial wires lengths. The ASP method's flowchart is presented in Fig. 14, and developed according to the two following procedures [135]:

i. The first column of the ASP's puzzle is shifted by 2. Succeeding columns are kept unique by shifting their corresponding previous columns by 2. Rows on the other hand are shifted by 1, until the stopping criteria is met.
ii. The established patterns in ASP puzzle must ensure that no sub-arrays would have the same numbering.

The drawback of ASP method is its need for skilled physical labors when selected for a real implementation in PV systems and impose additional wiring losses when compared to EAR technique [135].

Concerning different puzzle-based PV array reconfigurations, Table 3 records a comparative assessment of various techniques used in static PVR.

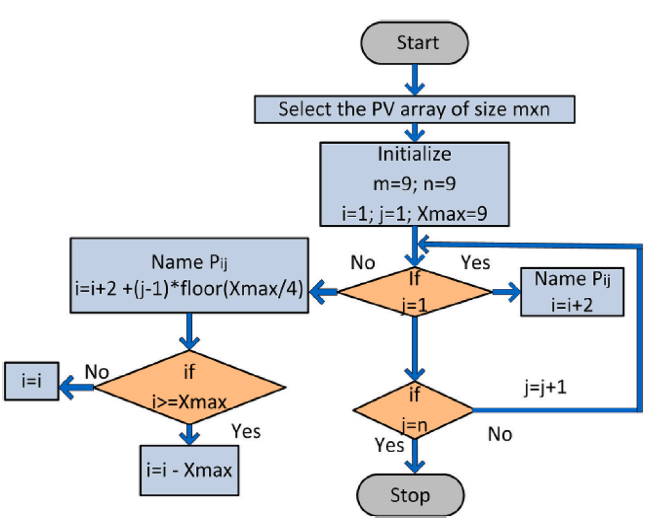

Fig. 14. Arithmetic Sequence Pattern method's flowchart [135].

Table 3
Comparison between different puzzle-based PVR methods.

Method	Advantages	Disadvantages
SuDoKu	• Ensures shade dispersion all over the array • Reduces mismatch losses	• Efficiency is related to the initial choice of SuDoKu pattern • Improper choice of the pattern could result in a reduced power output
Improved SuDoKu	• Reduces line losses • Increases dispersion factor	• Number repetition is seen in some of the sub-arrays • Can work optimally only for a 9 × 9 puzzle
Competence square	• Enhances power generation by up to 24.4% • Lowers power losses by up to 49%	The method was not investigated for various shading patterns such as random, diagonal, etc.
Skyscraper	• Applicable to any PV array size • Able to disperse all shading patterns	Presents difficulty in identifying accurate initial guesses
Magic square	• Decreases power losses • Develops a high fill factor	The method can withstand errors while adapting a higher than 4 × 4 PV array size
Dominance square	Similar to the advantages of CS	The diagonal reshaping gets harder with increasing PV array size
Futoshiki	Enables row shading dispersion into many rows	May include many inequality signs such as empty cells, number repetition, etc.
Latin square	• Power is enhanced by 6.81% compared to SuDoKu • Wiring loss is decreased by 18.86% compared to SuDoKu	In some shading patterns, the SuDoKu method achieves better fill factor than this method
KenKen	Increases output power while decreasing wire losses	A difficult mathematical model is behind the square's numeration
ZigZag	General improvement of PV operations under PSCs	Applicable to only small PV arrays.
AdDoKu	Superior performance compared to SuDoKu	Lacks real experimentation, and actual results' measurements
ACMS	Better than most other puzzle-based methods	Shading tests' conditions are very narrow
ASP	Possess a high power gain	Impose additional wire losses

Number based

Odd-Even (O-E). Each PV module of the array is labeled as M_{ij} with i, j denoting the number of row and column respectively [136]. Considering a 4 × 4 array, the arrangement starts by placing the modules with odd numbered row and odd numbered column in the first row. In succession, modules with even numbered row and even numbered column, are placed in the second row. Consecutively, the modules with odd numbered row and even numbered column are placed in the third row. Finally, the modules with even numbered row and odd numbered column are placed in the fourth row. This rearrangement process can be

M_{11}	M_{13}	M_{31}	M_{33}
M_{42}	M_{22}	M_{44}	M_{24}
M_{12}	M_{32}	M_{14}	M_{34}
M_{41}	M_{21}	M_{43}	M_{23}

Fig. 15. Odd-Even PVR [136].

visualized in Fig. 15.

The usage of this method has resulted in an increased power output by bypassing row currents, while reducing the existence of multiple peaks in P-V characteristic curve [136].

Odd-Even-Prime (O-E-P). As a way to increase PV power generation from the Odd-Even method in [136], the Odd-Even-Prime method decreases the mismatch losses and power losses due to hotspots formation, by decreasing the difference between maximum and minimum Sum of Irradiance (SIR) [137]. With the ability of application to any array size, the PV modules are relocated within the PV array according to the following steps [137]:

1. Placement of odd numbered row/column modules
2. Placement of even numbered row/column modules
3. Placement of prime numbered row/column modules
4. Placement of even numbered row and odd numbered column modules
5. Placement of odd numbered row and even numbered column modules
6. Placement of prime numbered row and odd numbered column modules
7. Placement of odd numbered row and prime numbered column modules
8. Placement of even numbered row and prime numbered column modules
9. Placement of prime numbered row and even numbered column modules

Row/Column index (RCI). The initial 9 × 9 matrix is decomposed into nine 3 × 3 matrices, and the relocation process is held for each sub-array by adding the row/column indices of panels [138].

Each obtained number represents the shifting place for the correspondent panel accordingly. For example, the panel P_{11} which is located at first row, first column, results in an index of two. Consequently, this panel is shifted two places downward. Different sub-arrays will follow the same procedure, ending up with total PV reconfiguration [138]. Among different number-based PVR, this method adapts the simplest mathematical form.

Nature inspired

Symbolizing the scroll of a river as an essential part of the ancient spiritual life, by means of old nine hall diagram, the Lo Shu (oldest matrix originated from ancient China) technique can be linked to enhanced PV power outputs [139]. The scrolling river indicates the PV panels' movement for a better shade dispersion. The correspondent sequential flowchart of Lo Shu method is described in the following three steps [139]:

1. Identification of Lo Shu mother matrix: the resulting first 3 × 3 sub-matrix of the total 9 × 9 matrix is rearranged as mother Lo Shu matrix
2. Column shift: in which the matrix' forward column shift is executed
3. Row shift: done for the previously shifted first three columns

Lo Shu technique minimizes row current differences, thus enhancing PV power output. Its procedural steps are simple, yielding in shade scattering with few panel movements [139].

Symmetry based

For a 5 × 4 PV array, PV panels are relocated according to Non Symmetrical (NS) patterns denoted as NS1 and NS2 [140]. The configurations NS1 and NS2 are only possible for patterns with odd-numbered rows. In case of repositioning only even-numbered rows, there would be a single NS pattern. The modelled 5 × 4 PV array has its first column filled in digits from 1 to 5 in ascending order. The first three rows of the second column add 2 to the digits in the same previous row/column, except for the last two rows, corresponding to numbers 1 and 2 respectively. Third column adds two to the previous column's numbers, except for rows 2 and 3. The final fourth column adds 2 to the number of the previous column, except for first and last rows. The determination process of the row and column (i, j) for NS1 and NS2 configurations are interpreted in Eqs. (19) and (20) respectively.

$$i = \begin{cases} i if j = 1 \\ i + (j-1) \times floor\left(\frac{i_{max}}{2}\right) if j > 1 \\ if i < i_{max}, i = i \\ else i = i - i_{max} end \end{cases} \tag{19}$$

$$i = \begin{cases} i if j = 1 \\ i + (j-1) \times ceil\left(\frac{i_{max}}{2}\right) if j > 1 \\ if i < i_{max}, i = i \\ else i = i - i_{max} end \end{cases} \tag{20}$$

The NS PV array reconfiguration enhances the PV output power, and better reduce losses due to shading, compared with other static PVR methods [140], but is less efficient for large arrays, and its wiring mode is complicated. This method's performance is ameliorated using Parity-Column Index (P-CI) strategy [141], where Eqs. (19) and (20) are improved in order to reconstruct the first row's position, as well as to define other row arrangements with different constraints. Entire rows are parity-grouped, along with specific vertical and transverse parity shifts, P-CI seemed effective in reducing wiring complexities seen in [140], with higher fill factor than other PVR techniques [141].

Distance maximizing

By physically relocating the PV panels within an array as far as possible from each others, while modifying their corresponding row/column positioning, the shadow pattern affecting the PV system can be distributed all over the array, thus increasing its energy outcomes [143].

After the panels' row/column rearrangement, a shifting process is introduced to reduce the concurrence between shading inducers and PV modules as seen in Fig. 16.

Although this technique minimizes the need for protection diodes and eliminate the occurrence of multiple local peaks in the P-V characteristic curve, it does not take into consideration the area restriction complexity, which PV systems generally suffer from.

Algorithm based

Static Shade Dispersion Physical Array Relocation (SD-PAR).

The SD-PAR algorithm proposes a 3 × 3 PV array repositioning according to the five steps summarized in Table 4 [144].

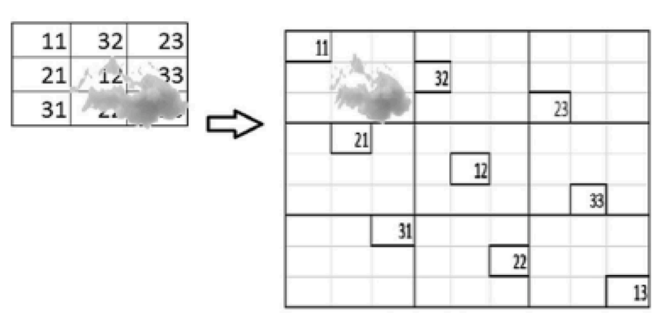

Fig. 16. Physical repositioning of PV panels based on distance maximizing [143].

Table 4
Executive steps for SD-PAR algorithm.

Step	Procedure
1	The matrix A is inputted having $m \times n$ as numbers of rows and columns respectively
2	Reset the value of the counter variable c to zero
3	While decreasing the value of the row variable i from n to one, increment c by 1, where the i^{th} column of the PV array is circularly shifted by c. Upon each increment, the value stored inside the variable d is horizontally concatenated then stored in the third column of the new PV array matrix B
4	Re-execution of the second iteration of the proposed algorithm
5	The value in matrix d is horizontally concatenated and stored in B

The resulting reconfiguration for the 3 × 3 PV array is exposed in Fig. 17.

This relatively simple, one time PVR, is found able to consequentially improve the output power under all shading conditions [144].

Static Shade Dispersion Positioning (SDP). The partial shading effect on a row, is dispersed over the entire PV array, where physical relocation of PV panels is condemned according to the following four steps [145]:

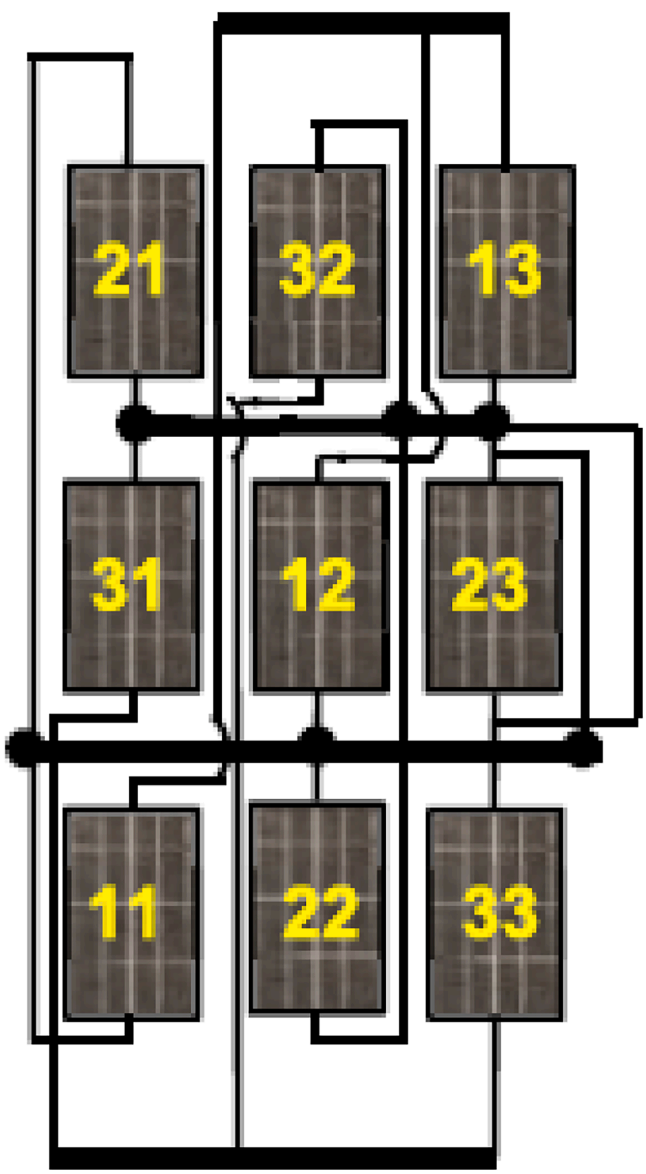

Fig. 17. SD-PAR reconfigured PV array [144].

Calculate the total number S of modules connected to the PV array.
Calculate the value of the real number $Z = \lfloor\sqrt{S}\rfloor$.
Check conditions when number of rows equals or not to the number of columns and rearrange the PV array accordingly.
When number of rows is different than number of columns, several increments/decrements by one, take place for numbers of rows/columns in order to create the modified PV array configuration.

When applied, this method better enhances the power production in a PV array, under various shading conditions, as compared to SuDoKu [145].

Electrical reconfiguration methods

The electrical (dynamic) PV array reconfiguration methods, are processes which continuously investigate the occurring shading patterns, and re-adapt the array accordingly, by means of switches and moveable electrical interconnections [146]. Different classifications for the surveyed electrical PVR techniques are recapitulated in Table 5.

Basic electrical interconnections

A single PV module's output power is limited due to its high dependence on environmental conditions, and its non-linear performance. Furthermore, parallel connected PV modules are more resilient as compared to series branches in front of PSCs (according to KCL). In contrast, series connected PV modules, offer bigger output voltage (according to KVL). Hence, panels are combined in series, parallel, and combination of Series/Parallel (SP) [147] for an optimized output power, as seen in Fig. 18.

The expansion of precedent interconnection schemes can be seen in Total Cross Tied (TCT), Honey Comb (HC) and Bridge Link (BL) circuit configurations [148]. Fig. 19 groups different expanded electrical interconnection for PV modules.

The Series-Parallel (SP) configuration shown in Fig. 18, takes advantage of current summation (from different branch currents in parallel connections), and voltage summation (from different series voltages). The TCT connection reduces the mismatch under uniform irradiance conditions when compared to SP. The BL scheme in turn, reduces cable losses and wiring's costs, since about half of the wires in TCT are avoided [149]. For most PV systems' configurations, TCT is more commonly used, due to its simplicity of execution and energy effectiveness [150].

Such electrical reconfiguration methods alter only the

Table 5
Major classification of electrical PVR.

Electrical PVR method	Description
Basic electrical interconnections	Involve basic wiring configurations for PV panels, such as series, parallel, honey comb, etc.
Improved electrical interconnections	The basic electrical interconnections are mutually hybridized with each others, to grant advantages from each. This involves series parallel mixed with bridge link, bridge link with honey comb, etc.
Algorithm based with/without embedded systems	The rules of reconfiguring electrical wirings are dictated by instructions' sets. Including full systems with algorithms executing on the actuators level, by switching on/off PV panels banks according to pre-defined conditions. This involves switching matrix, etc.
Artificial intelligence	Includes self-learning programming techniques which improve the PVR method's operational behaviors according to previous experiments
Hybrid	Includes two or more differently categorized methods within a single approach, such as electrical array reconfiguration mixed with a fuzzy logic controller operated under artificial neural network, etc.

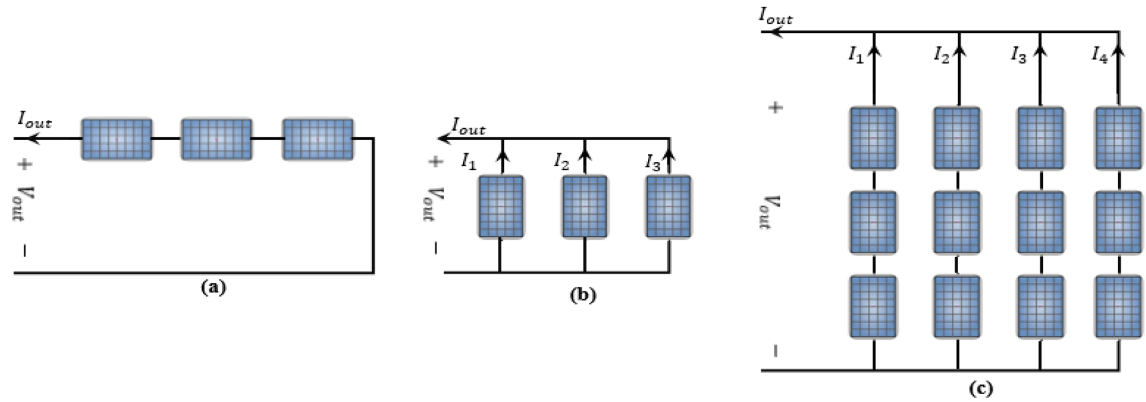

Fig. 18. Electrical interconnections (a) series (b) parallel (c) series–parallel.

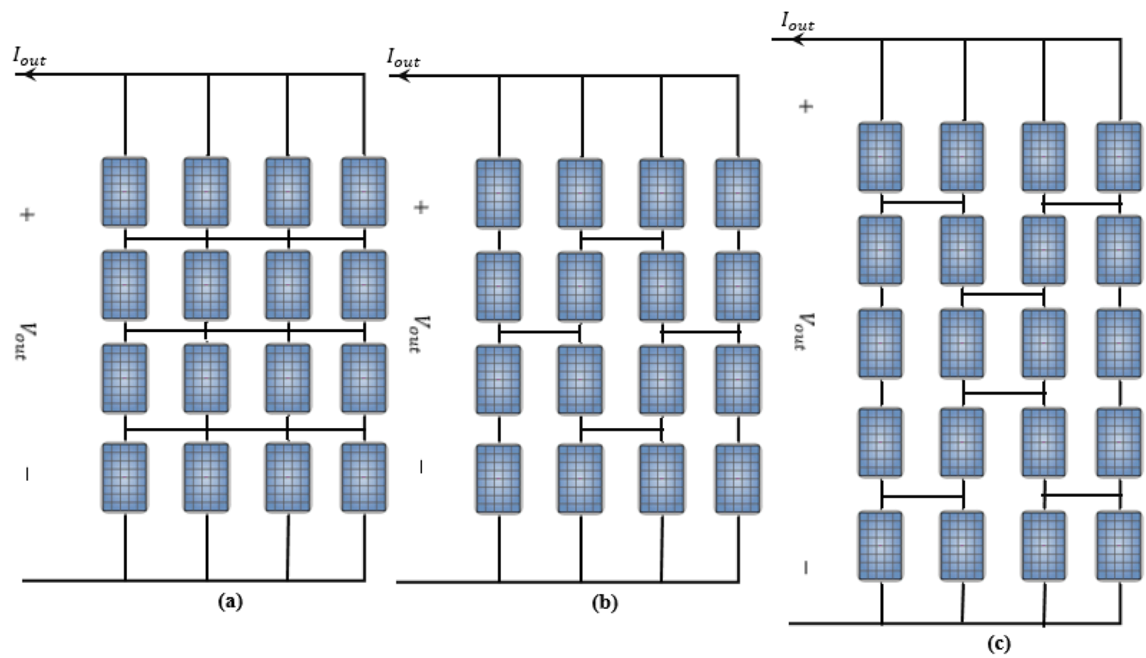

Fig. 19. Expanded electrical interconnections (a) Total-Cross-Tied (b) Honey Comb (c) Bridge Linked.

interconnections between the modules, without any dynamical switching in/off any part of the PV array.

Improved electrical interconnections

As a way to overcome the disabilities of conventional electrical interconnections, such as SP, TCT, BL, and HC, their modified rearrangements, such as Rearranged TCT (RTCT), Rearranged SP mixed with TCT (RSP-TCT), Rearranged BL mixed with TCT (RBL-TCT) and Rearranged BL mixed with HC (RBL-HC) yield in minor power losses. These configurations are presented in Fig. 20 [118].

Algorithm based with/without embedded systems

Mixed Integer Quadratic Programming (MIQP). Centered on branch and bound algorithm, the Mixed Integer Quadratic Programming (MIQP) improves a PV system's operational behavior under PSCs, by minimizing the Irradiance Mismatch Index (IMI). In other words, this dynamical reconfiguration of PV modules, reduces the sum of the differences' squares between normalized rows' irradiances. Such a process can take place after the formalization of the existence variable y_{iq} which is used in minimizing the objective function. This algorithm yields in defining a relocation process for shaded modules in both a Half Reconfigurable PV Array (HRPVA) and a Full Reconfigurable PV Array (FRPVA). The modules' repositioning process, in turns, is executed by means of 'm' number of switches, categorized as double-poled, multi-throws [151].

Population-Based algorithms (PBA). The set of Population Based Algorithms (PBA) includes the Flow Regime Algorithm (FRA), the Social Mimic Optimization Algorithm (SMOA) and Rao Optimization Algorithm (ROA) [152]. First and foremost, the FRA process relies on laminar and turbulent profiles of flowing fluids, where the exploitation and exploration phases are described by laminar and turbulent flows respectively. A Search Type Factor (STF) is used to achieve a balance between these two phases, as indicated in Eq. (21) [152].

$$STF_i = 3.2 \times 10^6 \times \frac{T_{max}}{n_t} \times \frac{||g^*_{n_t} - Z_i||}{||Z_j - Z_k||} \tag{21}$$

with $g^*_{n_t}$ denoting the global best solution, n_t the present iteration number, T_{max} the maximum number of iterations and Z_i, Z_j and Z_k the particles with the numbers i,j and k respectively. The STF comparison with the scalar 3.2×10^6 orientates the succeeding stage movement towards diversification or intensification.

Secondly, the SMOA bases on human expressions and body signals,

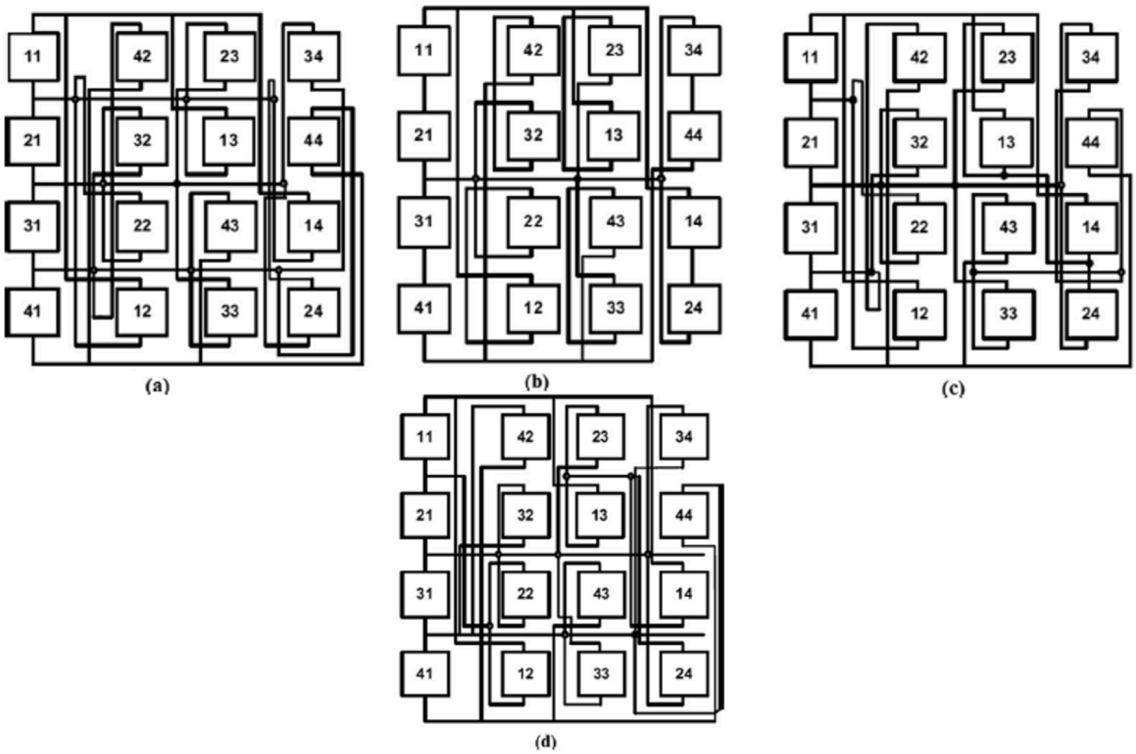

Fig. 20. Rearranged basic electrical interconnections (a) RTCT (b) RSP-TCT (c) RBL-TCT (d) RBL-HC [118].

in which the solution vector is updated according to the difference function between the individual and last iteration optimum solutions, as can be seen in Eq. (22) [152].

$$f_{Diff_{nt+1}} = \frac{\left(g^*_{n_t} - objectivefunction(Z_{i_{nt}})\right)}{objectivefunction(Z_{i_{nt}})} \tag{22}$$

where $g^*_{n_t}$ represents the global best solution, $Z_{i_{nt}}$ the solution vector of the i^{th} particle at iteration n_t and *objectivefunction* denoting the implemented fitness function.

Finally, the ROA, inspired from a new trend in population-size based optimization algorithm, depends on best/worst solutions resultant during the optimization process, in addition to random functions for solutions interconnections as explored in Eq. (23) [152].

$$Z_{i_{nt+1}} = Z_{i_{nt}} + rand_1\left(g^*_{nt} - |l^*_{nt}|\right) + rand_2\left(|Z_{i_{nt}}| - Z_{j_{nt}}\right) \tag{23}$$

with $Z_{i_{nt}}$ and $Z_{j_{nt}}$ representing the solutions of i^{th} and j^{th} candidates solutions respectively, $rand_1$ and $rand_2$ indicating randomly selected numbers from the interval [0;1] and g^*_{nt}, l^*_{nt} corresponding to best and worst solutions respectively at n_t iteration.

These three algorithms under the population based set, succeed over other PVR methods such as TCT and CS. The FRA algorithm has achieved the most superior performance and highest power enhancement among all, with 13% higher power generation than TCT [152].

Grasshopper Optimization algorithm (GOA). The Grasshopper Optimization Algorithm (GOA), with its simplicity and fewer requirements of controlling parameters, is able to reconfigure PV arrays according to the following six steps [153]:

1. Initialization of the controlling parameters of the algorithm with the correspondent PV array size
2. Construction of swarm matrix, where its number of rows/columns represent the number of search agents, and the dimension of the problem respectively
3. Application of the swarm matrix onto the PV array
4. Fitness function calculation, which represents the summed powers extracted from each given row as stated in Eq. (24)

$$\max(J) = \sum_{k=1}^{i}(V_k \times I_k) + (w_e/E_e) + (w_f \times P_a) \tag{24}$$

with i representing the rows' number, V_k, I_k the voltage and current at k^{th} row of the array respectively, P_a the panel's output voltage without bypass diodes, E_e the error of currents summation and w_e, w_f the weighting factors of E_e and P_a accordingly.

5. Removal of non-achieving constraint agents from the swarm
6. Finishing the algorithm if the difference error between the final fitness function and the precedent one is acceptable

The proposed GOA has enhanced the PV power output from 3.361% to 6.748% as compared to other PVR techniques such as TCT, SuDoKu and Genetic Algorithm (GA) [153].

Butterfly Optimization algorithm (BOA). Inspired by the food searching and mating processes followed by butterflies, the Butterfly Optimization Algorithm (BOA) exhibits a three staged mechanism, that would be later on employed for an optimal PVR solution, as follows [154]:

Initialization: in which the initial objective function is calculated, after a random formulation of butterflies' positions.

Iteration: here the fitness function f is calculated, after updating the butterflies' positions, as shown in Eq. (25).

$$f = cI^a \tag{25}$$

with c as the sensory fragrance, I as the stimulus' intensity and a a power

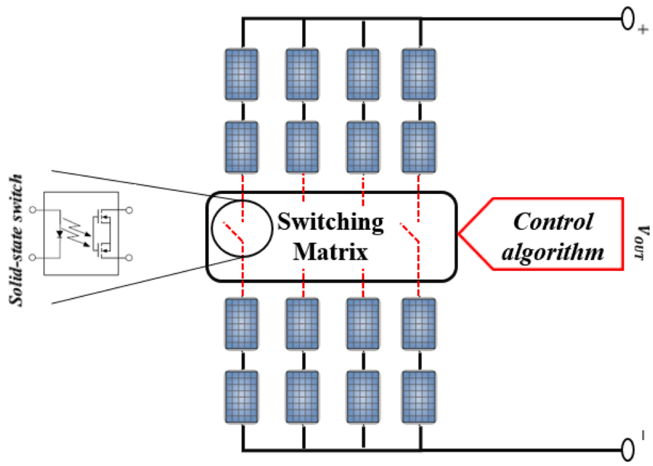

Fig. 21. PV switching matrix used in EAR.

exponent. Afterwards, during the first (global) search phase, the butterfly's position is updated towards the best global solution as shown in Eq. (26).

$$x_i^{t+1} = x_i^t + f_i(r^2 g^* - x_i^t) \quad (26)$$

with x_i^t representing the i^{th} butterfly at iteration t, f_i the fragrance of the i^{th} butterfly, r a random number within the interval [0;1] and g^* the current best global solution. On the other hand, the remaining local search can be expressed as in Eq. (27).

$$x_i^{t+1} = x_i^t + f_i(r^2 x_j^t - x_k^t) \quad (27)$$

with x_j^t and x_k^t denoting the j^{th} and k^{th} butterflies from the search space respectively.

Final stages: The stopping conditions are met, and the optimal solution is obtained.

The proposed BOA enhances the PV power productivity by 27.43% when compared to an SP-TCT arrangement. This algorithm, however, may suffer from delayed operations when implemented in hardware [154].

Munkres' Assignment algorithm (MAA). The usage of Munkres' Assignment Algorithm (MAA) allows a PVR with a minimum number of switching modules, thus increasing the lifetime of the Switching Matrix (SM) of a dynamic reconfiguration system [155].

The MAA sequential flowchart can be investigated according to the following steps:

Calculation of row irradiances' sum.(avg)
In the new matrix B, rows contain elements whose irradiances' sum is equal (or close) to.avg
Use MAA to find the minimum number of switching modules.
The matrix B is suitably re-arranged.

The MAA produces an optimum dynamic PVR, with delayed switches ageing processes [155].

Electrical array reconfiguration (EAR). By utilizing the irradiation data

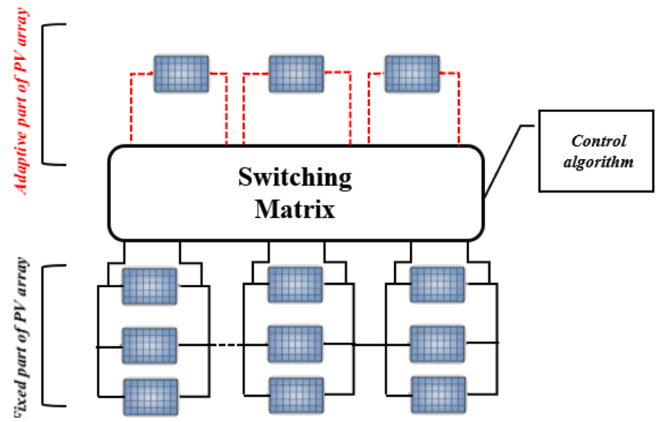

Fig. 22. Adaptive array reconfiguration method circuitry.

from Data Acquisition System (DAS), the Electrical Array Reconfiguration (EAR) allows a suitable modules repositioning based on irradiation levels and row currents [156]. The switching matrix shown in Fig. 21, is configured by means of computerized control systems (FPGA, DSP, etc.) where it would generate the switching states between PV modules [157].

With repetitive on/off switching mechanisms, governed by the present shading conditions, the connections between the PV modules are dynamically changed. This would offer a continuous monitoring of the shading patterns, thus enhancing a case-specified power production under different PSCs.

This method requires a fully reconfigurable array, with intensive need of sensors and switches, the fact that would decreases the PV system's cost efficiency [158].

Adaptive array reconfiguration (AAR). With a similar approach to mitigate the effects of PSCs over PV arrays as seen in EAR, the Adaptive Array Reconfiguration (AAR) categorizes the panels into either fixed or adaptive. Consequently, the switching matrix, shown in Fig. 22, is installed between fixed and adaptive parts, thus reducing rows' irradiance differences with a controller [159].

The AAR overcomes the drawbacks of EAR, by requiring less number of switching devices and sensors.

Modified Harris hawks Optimizer (MHHO). To avoid premature converging to local solutions in Harris Hawks Optimizer (HHO) [160], the Modified Harris Hawks Optimizer (MHHO), presented in reference [161] improves the exploration strategies, while reducing the escaping distribution over the number of iterations. The MHHO functions under two modified stages.

In the first stage, the global search is boosted during the modified exploration phase: the misleading zigzag motion of the prey is eliminated, by hawk's detection via Lé'vy flight (a probability distribution), as indicated in Eq. (28).

$$U(t+1)_i = U_m(t) + L\acute{e}'vy(D)\left(U_{prey}(t) - U(t_i)\right), P < 0.5 \quad (28)$$

with U_m denoting the mean position, U_{prey} the position of the prey, $U(t_i)$ the location vector in current iteration t_i and P a switching factor.

In the second step, the hawk's position is upgraded with reference to the average distance between three other random hawks, as shown in Eq. (29).

$$U(t+1)_i = \frac{\left(\left|U(t_i) - U_{rand_j}(t)\right| + \left|U(t_i) - U_{rand_k}(t)\right| + \left|U(t_i\right| - U_{rand_l}(t)\right)}{3} + U(t_i), P \geq 0.5 \quad (29)$$

with $U_{rand_j}(t), U_{rand_k}(t), U_{rand_l}(t)$ representing the randomly selected positions j, k, l for hawks from the population at iteration t.

The final stage of MHHO corresponds to evaluating the modified prey's energy equation, induced from the prey's fear of the predator, where it is noticed that a randomly shrinking exponential function is the most accurate in defining the rabbit energy, as expressed in Eq. (30).

$$E = 2E_0\left(2 \times rand \times exp^{-\left(\frac{\pi \times t}{2 \times T}\right)}\right) \quad (30)$$

with E representing the escape energy of the rabbit and E_0 a random variable inside the interval $[-1;1]$.

Under short/long-wide/narrows shading patterns, the MHHO showed a superior performance in determining the optimum interconnection for PV modules, when compared to other PVR methods such as HHO, TCT and CS [161].

Insulated Gate Bipolar Transistor model (IGBT model). A reconfiguration algorithm condemns the status of solid-state switches (Insulated Gate Bipolar Transistor (IGBT)), with a smart switching technique [162]. Each string within the PV array is set to be regrouped into two parallel strings: half of series-connected panels correspond to the modules in each string. Such process transforms the PV array dimensions into $(N_{S\_A}/2 \times 2N_{P\_A})$ where N_{S_A} and N_{P_A} represent the number of series panels in a string and the number of parallel strings respectively. Hence, conductors and converters' sizes can be reduced.

The MPPT algorithm, exposed in Fig. 23, tracks the GMPP simultaneously while calculating the optimum PV array reconfiguration. As a result, the reverse currents across shaded cells are reduced, where the entire model reflects a high reliability index. Still, this algorithm did not succeed in reducing reverse currents under all studied shading patterns [162].

Artificial intelligence

Rough Set Theory (RST). This artificial intelligence based technique, the Rough Set Theory (RST), has the ability to represent the conceptual similarities between the data of a given set, by grouping the corresponding similar values, and managing the relation between data, based on their intrinsic meaning [163].

Upon each submitted situation, the RST possesses a strong ability in decision making, according to the following logical flow chart, described in three steps:

Equivalence relation: The division of a given set of data into smaller subsets (equivalence classes), takes place as described in Eq. (31).

$$[u_i]R \bigcap_{\substack{i=1 \\ j \neq i}}^{n} [u_j]R = \varnothing \quad (31)$$

with $[u_i]R$, $[u_j]R$ representing the equivalence classes for indexes i and j and R a relation rule defining the relation between all elements of a given equivalence class. The intersection of all equivalent classes belonging to R is adapted as an equivalence relation.

Reduction of knowledge: This step ensures that the knowledge about a universe of objects is neither too insufficient nor too excessive.

3. Knowledge representation: by means of an Information System (IS), consisted of a tabulated data, the information is manipulated, to form a decision table as expressed in Eq. (32).

$$T = (U, A, C, D) where C \subseteq A and D \subseteq A \quad (32)$$

with U, A, representing universe and attributes sets respectively, and C, D representing conditions and decisions attributes respectively.

With simple logic circuits, an Automatic Reconfiguration System (ARS) is obtained after RST, through computer simulation, where the energy produced by shaded PV modules is better utilized [163]. However, this method is complex and requires heavy measurements.

Rule Based Fuzzy Approach (RBFA)

In order to reconfigure modules within a PV array, a Rule Based Fuzzy Approach (RBFA) is formulated by utilizing shading degree and irradiance derivative as control variables for designing fuzzy rules [164]. The approach starts by checking for partial shading by noticing the difference in the output voltage of each row.

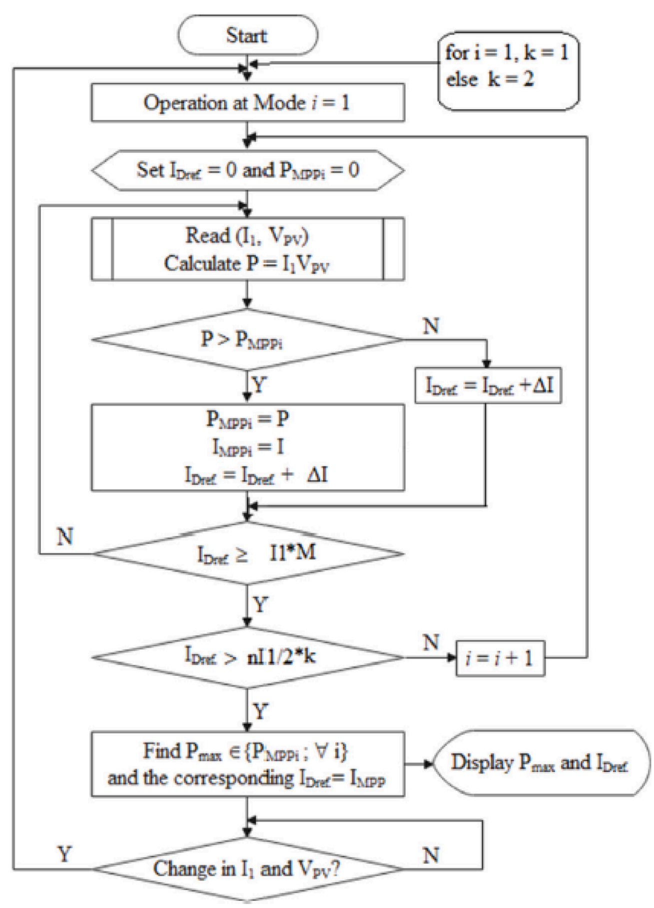

Fig. 23. Proposed MPPT and switching algorithm [162].

After the occurrence of a PSC, the shading degree is calculated according to Eq. (33).

$$\Delta G_{F_i} = G_{F_0} - G_{F_i} \quad (33)$$

with G_{F_0} and G_{F_i} denoting the irradiance on the non-shaded and other submodule respectively.

The obtained shading degree of each submodule and the derivative of irradiance are the input to the fuzzy controller, where after the fuzzification process, the output control is obtained. The PV array is finally rearranged after the fuzzy controller closes some switches of the matrix [164]. This method can be judged as non-reliable, since threshold based switching by a fuzzy controller does not accurately generate the switching matrix at dynamic irradiation conditions.

Hybrid

Series-parallel with binary coding (SPBC)

A binary coding has shown the potential of detecting PSCs. The

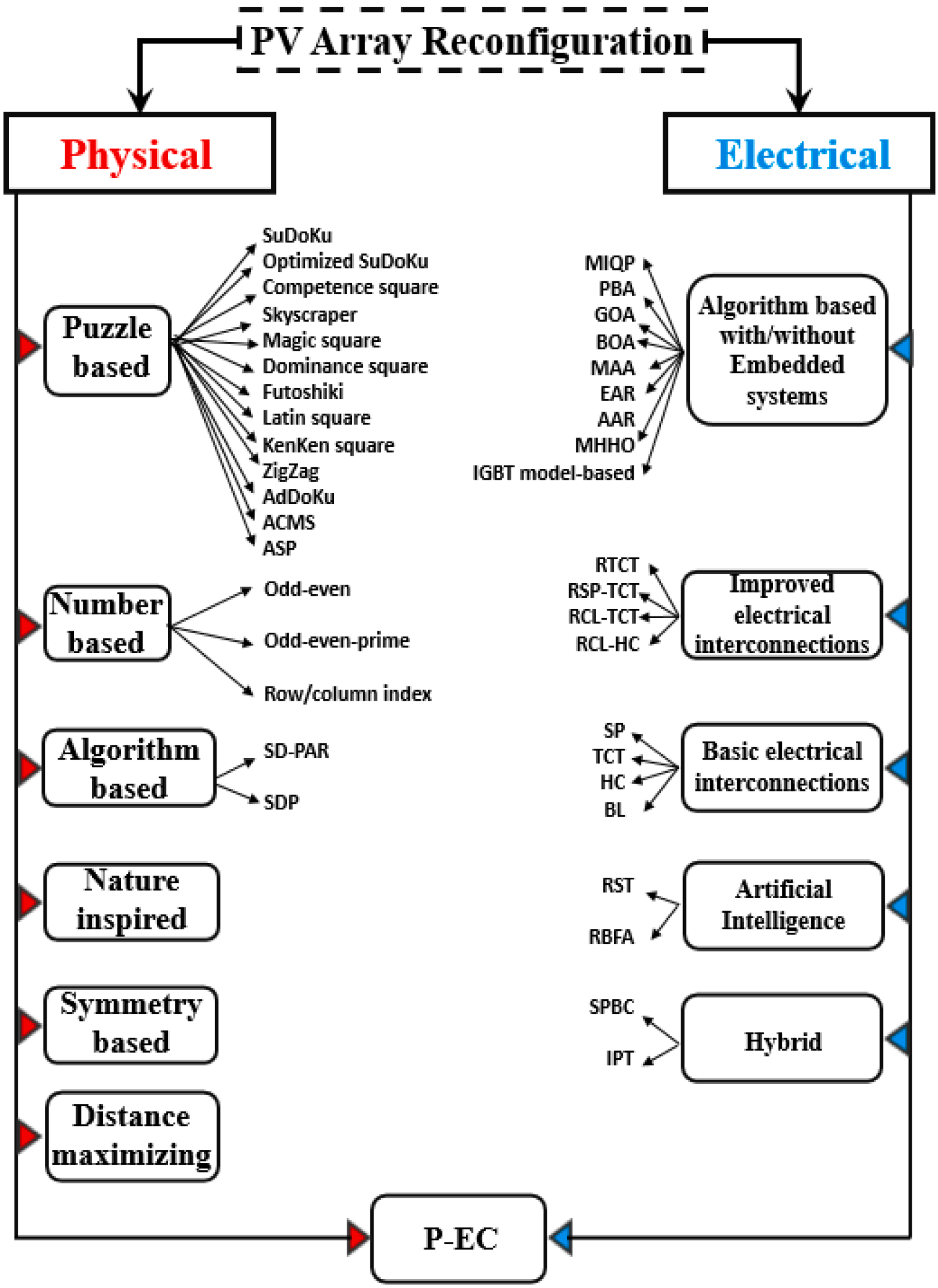

Fig. 24. Summary of all physical/electrical based PV array rearrangement methods.

combination of binary coding with conventional electrical reconfiguration methods (series, parallel, etc.), results in a PVR with superior efficiency as compared to standalone basic electrical interconnections [165]. A 3 × 3 PV array has its modules connected with a 9-bit binary up-counter, which produces a five hundreds twelve different states reflecting the shading scenarios from full shadow to full sun.

The choice of the best PVR is done after analyzing each reconfiguration according to its Power Generation Index (PGI) shown in Eq. (34).

$$PGI = \sum_{k=0}^{k=2^n-1}\left(\frac{1}{n}\right)\left(\frac{1}{2^n}P_k\right) \quad (34)$$

with n denoting the number of modules in the array, and P_k the maximum output power for each code of shadow (binary representation from 000000000 to 111111111).

The Series-Parallel Binary Coding (SPBC) can detect abnormalities in the produced currents, after adaptation of different reconfiguration patterns and definition of an average overcurrent value, for all codes of shadows. This would lead to an optimum choice for PVR pattern [165].

Image processing technique (IPT)

The AAR technique is hybridized with Image Processing Techniques (IPT) [166,167] which include a camera-centered system [168,169] that continuously monitors the shadow patterns on PV arrays [170]. The resulting image is afterwards submitted to an image processing unit. By means of a moving shadow detection algorithm, the control decision unit selects optimum panel layout according to image findings.

The process from image capture to algorithm output, passes through an image conversion to HSV (Hue Saturation Value) color space. The HSV in turn is filtered, undergoing through morphological process from erosion, dilation to blur. The shading rate is hence calculated according to the findings of black pixels. After comparison between the total frame and threshold times, the correspondent information is sent to the control unit, to finally dictate the on/off switching processes of the switching matrix. The application of IPT on a PV array, increases the MPP by up to 15% [170] but adds extra financial burden on the PV system's total cost.

Physical-electrical combined (P-EC). The P-EC (Physical-Electrical Combined) PVR strategy utilizes an enhanced configuration of the MS method, incorporated with an IE (Irradiance Equalization) strategy, applied for TCT arrays [171]. The dynamics of electrical interconnections are conducted via BCC-DPP (Bidirectional Cuk Converter-Differential Power Processing) unit, which in turn is controlled by MS-EC (Magic Square-Enhanced Configuration) algorithm.

Applied on a 6 × 6 TCT array, P-EC enhances the configuration of the conventional MS puzzle, by mixing 36 modules into 4 sub-TCT groups, each consisting of 9 modules, arranged into 3 ×3 TCT arrays. The IE algorithm in turn reduces the number of LMPP, thus directly targeting at GMPP. This is achievable by re-building the I-V characteristics for each PV module, where when added together, and overall I-V characteristics is obtained and stored within the best found maximum power, after several iterations [171].

The final destination of the proposed P-EC method takes place at the level of BCC-DPP unit, which is controlled by the developed IE algorithm. As output, P-EC offers a cross-connection function between PV chains, and the DC bus, resulting in power enhancements. The P-EC method is found flexible versus any shading pattern, however seemed extremely complex to construct [171].

After the expansion of each electrical-based PVR, it is clear that not all techniques involve a dynamical array rearranging. For instance, all basic and improved electrical interconnections are statically made, between electric terminals, rather in the geographical positioning of the entire module within the array. Dynamic reconfiguration methods are ones that involve a switching mechanism (switching matrix, etc.) to continuously reconnect/disconnect external PV modules to the array. To locate different found PVR methods, under physical, electrical, and combined categorizations, Fig. 24 points out all sub-methods corresponding to each set.

Discussion

The varieties of PVR methods, with different approaches, make it a hard choice for designers to adapt a standalone method, considered as the most optimum. In fact, the majority of the reviewed methods consider a cross connection between electrical and physical classifications: for example in reference [120], the SuDoKu based reconfiguration is applied for a TCT array. From another part, even within same PVR classification, the MIQP [151] and MAA [155] for example, are applied for TCT connected PV arrays.

The performance evaluation hence must be based upon a formulated scalar model, which underlies all techniques under the same mathematical aspects. The obtained results from different formulas give the chance to compare different rearranging methods, based on numbered evaluation criteria. Performance indices can be enumerated as Fill Factor (FF), Percentage Power Loss ($\%P_{Loss}$), Mismatch Power Loss (P_{ML}), Performance Ratio (PR), Execution Ratio (ER), Capacity Factor (CF), Efficiency (η), Percentage of Power Enhancement ($\%PE$) and outputted DC Power (P) [172,173].

The performance evaluation indices should also include a complexity index, to check how difficult the method is when implemented, and how many LMPPs exist in the characteristic P-V (Power-Voltage) curve after the implementation. Below are the mathematical expressions for different performance evaluation indices [172,173].

Fill factor: The ratio of the actual maximum power to the product of voltage and current in open-circuit, short-circuit respectively, represents the FF:

$$FF = \frac{V_{MP} \times I_{MP}}{V_{OC} \times I_{SC}} \quad (35)$$

such that V_{MP}, I_{MP} represent the maximum peak voltage and current respectively, and V_{OC}, I_{SC} the open-circuit voltage and short-circuit current respectively.

Mismatch power loss: The difference between power at unshaded condition and power at PSCs represents the $P_{MismatchLoss}$ as expanded in Eq. (36).

$$P_{ML} = P_{MAX_{unshaded}} - P_{GMPP_{PSC}} \quad (36)$$

with $P_{MAX_{unshaded}}$ and $P_{GMPP_{PSC}}$ representing the maximum power while no occurrence of any shading pattern and maximum power at PSCs respectively.

iii. Percentage power loss: the ratio of the global maximum peak at STC (Standard Test Conditions) subtracted from the global maximum peak at PSCs over the first denotes $\%P_{Loss}$ as indicated in Eq. (37).

$$\%P_{Loss} = \frac{GMPP_{STC} - GMPP_{PSC}}{GMPP_{STC}} \quad (37)$$

where $GMPP_{STC}$ and $GMPP_{PSC}$ represent global maximum peak at STC and global maximum peak at PSCs respectively.

iv. Performance ratio: a quality factor representing the amount of consumable solar energy as the ratio of the total energy generated by the array to the absolute power corresponds to PR as indicated in Eq. (38).

$$PR = \frac{EA}{P_{DC}} \quad (38)$$

with EA denoting the total energy generated by the array and P_{DC} the absolute power.

Execution ratio: The ratio of the maximum power generated at PSCs over the maximum power achieved at STC, represent the ER as expanded in Eq. (39).

$$ER = \frac{P_{PSC}}{P_{STC}} \quad (39)$$

where P_{PSC} and P_{STC} represent maximum power generated at PSCs and the maximum power achieved at STC respectively.

Capacity factor: It is the ratio of the actual energy produced E_{act} over the rated output power PV_{rated}, as indicated in Eq. (40).

$$CF = \frac{E_{act}}{PV_{rated}} \quad (40)$$

Efficiency: Corresponds to the ratio of global maximum peak power P_{GMPP} over input power P_{in} as indicated in Eq. (41).

$$\eta = \frac{P_{GMPP}}{P_{in}} \quad (41)$$

viii. Percentage of power enhancement: the ratio of the total power difference between conventional global power peak $GMPP_{conv}$ and case-specified global power peak $GMPP_{CS}$ over the power at conventional power peak is termed as $\%PE$, expanded in Eq. (42).

$$\%PE = \frac{GMPP_{conv} - GMPP_{CS}}{GMPP_{conv}} \quad (42)$$

ix. Outputted DC power: the output power P_{OUT} obtained at the PV array's terminals is shown in Eq. (43), with$k$ denoting a scalar smaller than one and V_M and I_M the maximum output voltage and current respectively.

$$P_{OUT} = k \times V_M \times I_M \quad (43)$$

In addition to Eqs. (35)–(43), the assessment of different PVR methods must take into consideration, their supportable shading patterns. From Table 1, the shading patterns are labeled as Random (R), Uneven Row shading (UR), Uneven Column shading (UC), Diagonal shading (D), Short and Narrow shading (SN), Short and Wide shading (SW), Long and Narrow shading (LN) and Long and Wide shading (LW).

Concerning all of these properties, Tables 6–9 present tabulated data for evaluating the performances of each of the PVR methods: the higher values of FF, PR, ER, η, %PE and P_{OUT} indicate a superior performance of the mentioned technique, as compared to others having lower values of the mentioned indexes. The ability of adapting different shading patterns within a method is a bonus. On the other hand, the high values of P_{ML} and $\%P_{Loss}$ reflect a foible for the method in use [176]. The most recent PVR techniques are encapsulated in Table 10 and are mutually compared to relevant older techniques. It is found that newer PVR methods are mainly centered over puzzle-based static category, where only a single research [171] hybridizes between electrical (initial circuit interconnections, with a dynamic computer-controlled re-arrangements) and physical schemes.

From another part the percentage of power enhancement in RST method is up to 84% [163] and 10% in IPT [170], where both RBFA [164] and SPBC [165] methods were seen easy to implement. Not all the methods presented in Tables 6–10, adapt the same shading patterns case studies, and concern the same PV array size: to standardize the comparison, the averaged values for each performance index were taken into consideration. Results shown in Table 10 clearly imply the need to concentrate on combined PVR strategies in future PVR research.

Conclusions and future work

The inescapable PSCs' traits accelerate the PV systems' aging process, while reducing their consumable output power, thus continuously decelerating the overall PV power generation's efficiency. As a solution, PVR methods show a good reliability when applied on PV systems, in terms of increasing their energy efficiency: by dispersing the shading pattern over the entire PV array, hence eliminating as much as possible

Table 6
Comparative assessment of physical puzzle based PVR methods.

Physical: Puzzle based	PVR methods	Shading patterns	Electrical properties FF	P_{ML}	$\%P_{Loss}$	PR	ER	η	%PE	P_{OUT}	Complexity	Number of LMPP	Refs.
	SDK	SW, LW, SN, LN	≤62.8	≈11%	–	–	–	≤20%	Up to 26.1%	Up to 63 V_MI_M	High	2	[115119]
	O-SDK	SW, LW, SN, LN	–	≈3%	–	–	–	≤20.6%	26.88%	–	High	–	[122]
	CS	SW, LW, SN, LN	≤53	≥3.08%	≥30%	–	–	–	Up to 24.4%	Up to 65.7 V_MI_M	High	1	[123]
	SS	LW, SN, SW	≤70.7	≈3.4%	≥30.5%	–	–	–	Up to 43.7%	Up to 64.8 V_MI_M	Medium	3	[124]
	MS	LW	90.9	–	≥14%	–	–	–	25.40%	Up to 48.6 V_MI_M	High	1	[125126]
	DS	All	≤65.4	≥2.5%	≥34.5%	–	–	≤90%	–	Up to 19 V_MI_M	High	3	[128]
	SS	SW, LW, SN, LN	–	–	–	–	–	≤88.5%	Up to 24.24%	Up to 21.6 V_MI_M	High	1	[129]
	FS	SW, LW, SN, LN	≤22.94	–	≥16.1%	–	Up to 84.50%	–	–	Up to 31.2 V_MI_M	High	2	[131]
	LS	SW, LW, SN, LN	≤64.7	–	–	–	–	≤10.9%	–	Up to 13.6 V_MI_M	High	1	[132]
	ZZ	LN, SN, LW, UR	≤70.5	≥0.44%	≥15%	≤0.92%	–	–	Up to 22%	Up to 10 V_MI_M	High	2	[142]

Table 7
Comparative assessment of Physical PVR: number based, algorithm based, nature inspired, symmetry based and distance maximizing based methods.

	PVR methods	Shading patterns	Electrical properties									Complexity	Number of LMPP	Refs.
			FF	P_{ML}	$\%P_{Loss}$	PR	ER	CF	η	%PE	P_{OUT}			
Physical: ***Number based***	O-E	SW, LW, SN, LN	–	≥1.03%	–	–	–	–		Up to 30.88%	Up to 13.2 V_MI_M	Medium	2	[136]
	O-E-P	SN	≤63.18	≥14.5%	–	–	–	–	≤11.3%	–	Up to 64.81 V_MI_M	Low	2	[137]
	RCI	SW, LW, SN, LN	≤81	≥24.1%	≥19%	–	–	–	–	–	Up to 63.9 V_MI_M	High	3	[138]
Physical: ***Algorithm based***	SD-PAR	All	–	–	–	–	–	–	≈ 99.4%	Up to 70%	–	Low	2	[145]
	SDP	SW, LW, SN, LN	–	–	–	–	–	–	≈ 98%	Up to 23.65%	Up to 6.6 V_MI_M	Medium	3	[145]
Physical: ***Nature inspired***		SW, LW, SN, LN	≤52.63	≥3%	≥31%	100%	≤91%	≤0.69	–	–	Up to 63 V_MI_M	Low	2	[139]
Physical: ***Symmetry based***		All	≤22	–	≥12.2%	–	–	–	–	–	Up to 16.75 V_MI_M	Medium	2	[140]
Physical: ***Distance maximizing***		SW, LW, SN, LN	–	–	–	–	–	–	≤90%	–	–	Low	1	[143]

Table 8
Comparative assessment of Electrical PVR: algorithm based methods.

Electrical: ***Algorithm based***	**PVR methods**	**Shading patterns**	**Electrical properties** FF	P_{ML}	$\%P_{Loss}$	PR	η	%PE	P_{OUT}	**Complexity**	**Number of LMPP**	**Refs.**
	MIQP	SN, LN, UR	–	–	–	Up to 1	–	Up to 41.6%	–	Medium	3	[151]
	PBA	LW, SN, LN	≤78.6	≥21.2%	≥18.6%	–	≈ 81.37%	Up to 28%	Up to 63.91 V_MI_M	High	2	[152]
	GOA	SN, SW, LN, LW	–	–	–	–	–	3.36%	Up to 65.71 V_MI_M	Medium	1	[153]
	BOA	UC, R, LW, LW	≤16.38	–	≥69.9%		–		Up to 20 V_MI_M	High	4	[154]
	MAA	All	–	–	–	–	–	–	–	High	1	[155]
	EAR	All	–	–	–	–	Up to 43%	Up to 31%	–	High	2	[156]
	AAR	All	–	–	≥0.06%	0.8675	–	–	–	Medium	4	[159]
	MHHO	SN, SW, LN, LW	≤75.9	≥18.7%	≥15.7%	–	Up to 78.37%	Up to 33.2%	Up to 82.2 V_MI_M	High	2	[161]

Table 9
Comparative assessment of Electrical PVR: improved and basic electrical interconnections based methods.

	PVR methods	Shading patterns	Electrical properties					Complexity	Number of LMPP	Refs.
			FF	P_{ML}	$\%P_{Loss}$	η	%PE			
Electrical: ***Improved electrical interconnections***	RTCT	All	≤75.2	≥7%	≥6.54%	Up to 13.9%	–	High	2	[174]
	RSP-TCT	All	≤70.44	≥11.7%	≥4.04%	–	Up to 6.59%	High	3	[175]
	RBL-TCT	All	≤70.77	≥11.2%	≥3.07%	–	Up to 7.55%	High	3	[175]
	RBL-HC	All	≤70.87	≥10.9%	≥2.49%	–	Up to 10.02%	High	2	[175]
Electrical: ***Basic electrical interconnections***	SP	All	≤68.30	≥14.3%	≥12.9%	–	–	Low	3	[175]
	TCT	All	≤71.48	≥10.6%	≥2.42%	–	Up to 19.58%	High	1	[175]
	HC	All	≤70.19	≥11.9%	≥3.73%	–	Up to 18.08%	High	2	[175]
	BL	All	≤68.76	≥12.7%	≥5.33%	–	Up to 8.04%	High	2	[175]

Table 10
Recent PVR methods.

Recent PVR method	Classification			Results	Refs.
	Physical	Electrical	Combined		
AdDoKu	✓ (puzzle-based)			• Better output power when compared to TCT by up to 30.15% • Power improvement by 1.94% when compared to SuDoKu • Lower line losses when compared to both SuDoKu (12.2%-36.8%) and TCT (19.5%-51.5%) • FF is the same as in SuDoKu	[133]
ACMS	✓ (puzzle-based)			• $\%P_{Loss}$ is decreased by 1.93% when compared to SuDoKu • FF has improved by 0.51% when compared to SuDoKu • 1.93 increment in PR when compared to SuDoKu • 7.15% power gain as compared to TCT	[134]
ASP	✓ (puzzle-based)			• Provides a maximum reduction of 37.98% in needed wires as compared to SS • FF is up to 71.5% • Up to 33.78% reduction in P_{ML} as compared to TCT • Recorded experimental power gain was up to 42.91% • Almost same efficiency as SuDoKu, FS, O-SDK, SS, and MS	[135]
P-CI	✓ (symmetry-based)			• P_{OUT} is up to $71.1 V_M I_M$ • FF is up to 69.3% • Largest $\%P_{Loss}$ is 29.1% smaller than one in O-E	[141]
IGBT model-based		✓ (algorithm-based)		• Highest $\%P_{Loss}$ was beneath 2.48% • Switching losses of IGBTs were at maximum of 2.34% as compared to ideal switch circuits	[162]
P-EC			✓	• Average power gain is up to 48% • Efficiency is up to 98.95%	[171]

any rows' currents differences. When compared to other PSCs mitigation techniques (i.e., MPPT, micro-inverters, etc.) PVR methods require less complexity/space for installation while still relatively ensuring a homogeneous power production across the PV array. This in turn reduces the hotspots creation probability and its consequences (i.e., burnouts, fire hazards, etc.).

Through this paper, PVR methods were characterized as either physical, electrical, or physical-electrical combined. Physical PVR techniques are based on PV modules' positioning adjustments within the array. This major set contains puzzle-based techniques (difficult to construct), number-based and symmetry-based methods (require complex circuit designs). Additionally, distance maximizing based techniques require extra spaces to be implemented, where Lo Shu based method imposes hard computational skills. Among various physical PVRs, the SD-PAR algorithm is resilient in front of all possible shading patterns, with an almost 100% efficiency and 70% power enhancement (Table 7).

On the other hand, electrical PVR techniques reshape the electrical interconnections between circuits' nodes, rather than dislocating the entire PV module from its place. As revealed from Table 9, the TCT circuit architecture is the most suitable configuration for PV arrays as it requires less wire demand when compared to HC and BL, RSP and other connections' arrangements. Minor power improvements were noticed upon the application of hybrid based electrical PVR, where artificial intelligence methods require difficult programming specialties. Among algorithm-based electrical PVR strategies, the MHHO algorithm produced the highest output DC power (82.2 $V_M I_M$), with a high fill factor (around 75%) and minimum power losses and power mismatch losses (around 16% and 19% respectively). The majority of the surveyed PVR methods, hybridize between electrical (with no SM) and physical sets, such as TCT-SuDoKu, TCT-KenKen, etc., where only a single method (P-EC) combines physical and electrical PVR (including switching devices) with a decision making algorithm for a dynamical PV modules' switching.

For a future PVR scope, the PV panels are first recommended to be TCT-configured, as a tradeoff between complexity and efficiency when compared to other electrical interconnections (i.e., RSP-TCT, RBL-TCT, R-TCT, etc.). Successively, the SD-PAR algorithm after different iterations, relocates (for only once) the TCT configured modules. At this level, the static reconfiguration process is done. After so, configured PV modules are to be interfered with an SM which in turn is controlled by the MHHO algorithm. Theoretically, this crossed configuration planning would have an efficiency near 100%, more than 75% power enhancement, with reduced mismatch and power losses to around 10% and 3% respectively, and a high fill factor around 80%. Such PVR scheme is encouraged to be experimentally investigated in real PV systems, in order to have discrete and quantitative results, which evaluates its effectiveness versus PSCs mitigation, and better PV power productivity.

Declaration of Competing Interest

The authors declare that they have no known competing financial interests or personal relationships that could have appeared to influence the work reported in this paper.

References

[1] A.G. Olabi, The 3rd international conference on sustainable energy and environmental protection SEEP 2009 – Guest Editor's Introduction, Energy 35 (12) (2010) 4508–4509.
[2] B.R. David, S. Spencer, J. Miller, S. Almahmoud, H. Jouhara, Comparative environmental life cycle assessment of conventional energy storage system and innovative thermal energy storage system, Int. J. Thermofluids 12 (2021), 100116.
[3] S. Abdo, H. Saidani-Scott, M.A. Abdelrahman, Numerical study with eco-exergy analysis and sustainability assessment for a stand-alone nanofluit PVT/T, Therm. Sci. Eng. Progress 24 (2021), 100931.
[4] K. Obaideen, M.N. AlMallahi, A.H. Alami, M. Ramadan, M.A. Abdelkareem, N. Shehata, A.G. Olabi, On the contribution of solar energy to sustainable developments goals: case study on Mohammed bin Rashid Al Makhtoum Solar Park, Int. J. Thermofluids 12 (2021), 100123.
[5] S. Mehranfar, A. Gharehghani, A. Azizi, A.M. Andwari, A. Pesyridis, H. Jouhara, Comparative assessment of innovative methods to improve solar chimney power plant efficiency, Sustain. Energy Technol. Assess. 49 (2022), 101807.
[6] A.H. Alami, M. Ramadan, M.A. Abdelkareem, J.J. Alghawi, N.T. Alhattawi, H. A. Mohamad, A.-G. Olabi, Novel and practical photovoltaic applications, Therm. Sci. Eng. Progress 29 (2022), 101208.
[7] N. Khordehgah, V. Guichet, S.P. Lester, H. Jouhara, Computational study and experimental validation of a solar photovoltaics and thermal technology, Renewable Energy. 143 (2019) 1348–1356.
[8] M. Venturelli, D. Brough, M. Milani, L. Montorsi, H. Jouhara, Comprehensive numerical model for the analysis of potential heat recovery solutions in a ceramic industry, Int. J. Thermofluids 10 (2021), 100080.
[9] V. Guichet, N. Khordehgah, H. Jouhara, Experimental investigation and analytical prediction of a multi-channel flat heat pipe thermal performance, Int. J. Thermofluids 5-6 (2020), 100038.
[10] H. Jouhara, A. Zabnienska-Gora, N. Khordehgah, D. Ahmad, T. Lipinski, Latent thermal energy storage technologies and applications: a review, Int. J. Thermofluids 5-6 (2020), 100039.
[11] F. Hengel, C. Heschl, F. Inschlag, P. Klanatsky, System efficiency of pvt collector-driven heat pumps, Int. J. Thermofluids 5-6 (2020), 100034.
[12] M. Rashad, N. Khordehgah, A. Zabnienska-Gora, L. Ahmad, H. Jouhara, The utilisation of useful ambient energy in residential dwellings to improve thermal comfort and reduce energy consumption, Int. J. Thermofluids 9 (2021), 100059.

[13] L. Ahmad, N. Khordergah, J. Malinauskaite, H. Jouhara, Recent advances and applications of solar photovoltaics and thermal technologies, Energy 207 (2020), 118254.
[14] K. Osmani, M. Ramadan, T. Lemenand, B. Castanier, A. Haddad, Optimization of PV array tilt angle for minimum levelized cost of energy, Comput. Electr. Eng. 96 (2021), 107474.
[15] K. Osmani, A. Haddad, T. Lemenand, B. Castanier, M. Ramadan, A review on maintenance strategies for PV systems, Sci. Total Environ. 746 (2020), 141753.
[16] O.K. Ahmed, Z.A. Mohammed, Dust effect on the performance of the hybrid PV/Thermal collector, Therm. Sci. Eng. Progress 3 (2017) 114–122.
[17] H. Wang, R. Cai, B. Zhou, S. Aziz, B. Qin, N. Voropai, L. Gan, E. Barakhtenko, Solar irradiance forecasting based on direct explainable neural network, Energy Convers. Manage. 226 (2020), 113487.
[18] A.H. Alami, M.K.H. Rabaia, E.T. Sayed, M. Ramadan, M.A. Abdelkareem, S. Alasad, A.-G. Olabi, Management of potential challenges of PV technology proliferation, Sustain. Energy Technol. Assess. 51 (2022), 101942.
[19] H.M. Ridha, Parameters extraction of single and double diodes photovoltaic models using Marine Predators Algorithm and Lambert W function, Solar Energy. 209 (2020) 674–693.
[20] H. Mohammed, M. Kumar, R. Gupta, Bypass diode effect on temperature distribution in crystalline silicon photovoltaic module under partial shading, Solar Energy. 208 (2020) 182–194.
[21] L. Papargyri, M. Theristis, B. Kubicek, T. Krametz, C. Mayr, P. Papanastasiou, G. E. Georghiou, Modelling and experimental investigations of microcracks in crystalline silicon photovoltaics: a review, Renewable Energy 145 (2020) 2387–2408.
[22] H.-D. Liu, C.-H. Lin, K.-J. Pai, C.-M. Wang, A GMPPT algorithm for preventing the LMPP problems based on trend line transformation technique, Solar Energy 198 (2020) 53–67.
[23] M.P. Bonkile, V. Ramadesigan, Physics-based models in PV-battery hybrid power systems: thermal management and degradation analysis, J. Energy Storage 31 (2020), 101458.
[24] C. Tubniyom, W. Jaideaw, R. Chatthaworn, A. Suksri, T. Wongwuttanasatian, Effect of partial shading patterns and degrees of shading on Total-Cross-Tied (TCT) photovoltaic array configuration, Energy Procedia. 153 (2018) 35–41.
[25] C.E. Clement, J.P. Singh, E. Birgersson, Y. Wang, Y.S. Khoo, Hotspot development and shading response of shingled PV modules, Solar Energy 207 (2020) 729–735.
[26] J. Zaraket, M. Aillerie, C. Salame, E. Losson, Output voltage changes in PV solar modules after electrical and thermal stresses. Experimental analysis, Energy Procedia 157 (2019) 1404–1411.
[27] S. Deng, Z. Zhang, C. Ju, J. Dong, Z. Xia, X. Yan, T. Xu, G. Xing, Research on hot spot risk for high-efficiency solar module, Energy Procedia 130 (2017) 77–86.
[28] M.L. Orozco-Gutierrez, J.M. Ramirez-Scarpetta, G. Spagnuolo, C.A. Ramos-Paja, A method for simulating large PV arrays that include reverse biased cells, Appl. Energy 123 (2014) 157–167.
[29] T. Ghanbari, Permanent partial shading detection for protection of photovoltaic panels against hot spotting, IET Renewable Power Generation 11 (1) (2016) 1–9.
[30] K. Mahmoud, M. Lehtonen, Three-level control strategy for minimizing voltage deviation and flicker in PV-rich distribution systems, Int. J. Electr. Power Energy Syst. 120 (2020), 105997.
[31] L. Ahmad, N. Khordehgah, J. Malinauskaite, H. Jouhara, Recent advances and applications of solar photovoltaics and thermal technologies, Energy 207 (2020), 118254.
[32] Z. Wang, N. Zhou, L. Gong, M. Jiang, Quantitative estimation of mismatch losses in photovoltaic arrays under partial shading conditions, Optik 203 (2020), 163950.
[33] M. Dhimish, V. Holmes, B. Mehrdadi, M. Dales, B. Chong, L. Zhang, Seven indicators variations for multiple PV array configurations under partial shading and faulty PV conditions, Renewable Energy 113 (2017) 438–460.
[34] D.P. Winston, S. Kumaravel, B.P. Kumar, S. Devakirubakaran, Performance improvement of solar PV array topologies during various partial shading conditions, Solar Energy 196 (2020) 228–242.
[35] I.H. Mahammed, A.H. Arab, S. Berrah, Y. Bakelli, M. Khennene, S.H. Oudjana, A. Fezzani, L. Zaghba, Outdoor study of partial shading effects on different PV modules technologies, Energy Procedia 141 (2017) 81–85.
[36] J.C. Teo, R.H.G. Tan, V.H. Mok, V.K. Ramachandaramurthy, C.K. Tan, Impact of bypass diode forward voltage on maximum power of a photovoltaic system under partial shading conditions, Energy 191 (2020), 116491.
[37] P. Bauwens, J. Doutreloigne, Reducing partial shading power loss with an integrated Smart Bypass, Solar Energy 103 (2014) 134–142.
[38] K. Lappalainen, S. Valkealahti, Number of maximum power points in photovoltaic arrays during partial shading events by clouds, Renewable Energy 152 (2020) 812–822.
[39] M.V. da Rocha, L.P. Sampaio, S.A.O. da Silva, Comparative analysis of MPPT algorithms based on Bat algorithm for PV systems under partial shading conditions, Sustain. Energy Technol. Assess. 40 (2020), 100761.
[40] K. Osmani, A. Haddad, T. Lemenand, B. Castanier, M. Ramadan, An investigation on maximum power extraction algorithms from PV systems with corresponding DC-DC converters, Energy 224 (2021), 120092.
[41] M. Mao, L. Cui, Q. Zhang, K. Guo, L. Zhou, H. Huang, Classification and summarization of solar photovoltaic MPPT techniques: a review based on traditional and intelligent control strategies, Energy Rep. 6 (2020) 1312–1327.
[42] O. Celik, A. Teke, A. Tan, Overview of micro-inverters as a challenging technology in photovoltaic applications, Renew. Sustain. Energy Rev. 82 (3) (2018) 3191–3206.
[43] Z.E.T. Ternifi, P. Petit, G. Bachir, M. Aillerie, New Topology of Photovoltaic Microinverter based on Boost converter, Energy Procedia 119 (2017) 938–944.
[44] R. Pachauri, R. Singh, A. Gehlot, R. Samakaria, S. Choudhury, Experimental analysis to extract maximum power from PV array reconfiguration under partial shading conditions, Eng. Sci. Technol. Int. J. 22 (1) (2019) 109–130.
[45] A. Hazra, S. Das, M. Basu, An efficient fault diagnosis method for PV systems following string current, J. Clean. Prod. 154 (2017) 220–232.
[46] H.N. Manjunath, S.R. Suresh, Reduction of mislead power and mismatch power loss under partial shading conditions using novel square matrix shade dispersion technique, Solar Energy. 207 (2020) 1364–1383.
[47] M. Matam, V.R. Barry, Improved performance of dynamic photovoltaic array under repeating shade conditions, Energy Convers. Manage. 168 (2018) 639–650.
[48] M. Horoufiany, R. Ghandehari, Optimization of the Sudoku based reconfiguration technique for PV arrays power enhancement under mutual shading conditions, Solar Energy 159 (2018) 1037–1046.
[49] X. Chen, Y. Du, E. Lim, H. Wen, K. Yan, J. Kirtley, Power ramp-rates of utility-scale PV systems under passing clouds: Module-level emulation with cloud shadow modeling, Appl. Energy 268 (2020) 114980.
[50] B. Mukhopadhyay, D. Das, Multi-objective dynamic and static reconfiguration with optimized allocation of PV-DG and battery energy storage system, Renew. Sustain. Energy Rev. 124 (2020), 109777.
[51] S. Xue, Q. Jia, S. Tian, Y. Su, H. Yu, Performance improvement strategy for photovoltaic generation through dynamic reconfiguration of cell strings, Int. J. Electric. Power Energy Syst. 125 (2021), 106456.
[52] P.R. Satpathy, R. Sharma, Reliability and losses investigation of photovoltaic power generators during partial shading, Energy Convers. Manage. 223 (2020), 113480.
[53] C. Dechthummarong, B. Wiengmoon, D. Chenvidhya, C. Jivacate, K. Kirtikara, Physical deterioration of encapsulation and electrical insulation properties of PV modules after long-term operation in Thailand, Solar Energy Mater. Solar Cells 94 (9) (2010) 1437–1440.
[54] M. Horoufiany, R. Ghandehari, An optimal fixed reconfiguration scheme for PV arrays power enhancement under mutual shading conditions, IET Renewable Power Generation 11 (11) (2017) 1456–1463.
[55] L. Idoko, O. Anaya-Lara, A. McDonald, Enhancing PV modules efficiency and power output using multi-concept cooling technique, Energy Rep. 4 (2018) 357–369.
[56] H. Hanifi, M.Z. Khan, B. Jaeckel, C. Hagendorf, J. Schneider, A. Abdallah, K. Ilse, Optimum PV module interconnection layout and mounting orientation to reduce inhomogeneous soiling losses in desert environments, Solar Energy 203 (2020) 267–274.
[57] O.W. Yen, B.C. Babu, Simple and easy approach for mathematical analysis of photovoltaic (PV) module under normal and partial shading conditions, Optik 169 (2018) 48–61.
[58] Y. Yang, K.A. Kim, T. Ding. 2018. Chapter 9 – Modeling and Control of PV Systems. Control of Power Electronic Converters and Systems. Academic Press. pp. 243-68.
[59] S.R. Pendem, S. Mikkili, Modeling, simulation and performance analysis of solar PV array configurations (Series, Series-Parallel and Honey-Comb) to extract maximum power under Partial Shading Conditions, Energy Rep. 4 (2018) 274–287.
[60] D. Yousri, S.B. Thanikanti, D. Allam, V.K. Ramachandaramurthy, M.B. Eteiba, Fractional chaotic ensemble particle swarm optimizer for identifying the single, double, and three diode photovoltaic models' parameters, Energy 195 (2020), 116979.
[61] D. Yousri, T.S. Babu, D. Allam, V.K. Ramachandaramurthy, M.B. Etiba, A novel chaotic flower pollination algorithm for global maximum power point tracking for photovoltaic system under partial shading conditions, IEEE Access 7 (2019) 121432–121445.
[62] D.P. Winston, B.P. Kumar, S.C. Christabel, A.J. Chamkha, R. Sathyamurthy, Maximum power extraction in solar renewable power system – a bypass diode scanning approach, Comput. Electr. Eng. 70 (2018) 122–136.
[63] A. Ndiaye, C.M.F. Kébé, A. Charki, V. Sambou, P.A. Ndiaye, Photovoltaic platform for investigating PV module degradation, Energy Procedia 74 (2015) 1370–1380.
[64] E.I. Batzelis, Simple PV performance equations theoretically well founded on the single-diode model, IEEE J. Photovoltaics 7 (5) (2017) 1400–1409.
[65] T.S. Babu, J.P. Ram, T. Dragicevic, M. Miyatake, F. Blaabjerg, N. Rajasekar, Particle swarm optimization based solar PV array reconfiguration of the maximum power extraction under partial shading conditions, IEEE Trans. Sustain. Energy 9 (1) (2017) 74–85.
[66] M.A. Awadallah, Variations of the bacterial foraging algorithm for the extraction of PV module parameters from nameplate data, Energy Convers. Manage. 113 (2016) 312–320.
[67] W. Charfi, M. Chaabane, H. Mhiri, P. Bournot, Performance evaluation of a solar photovoltaic system, Energy Rep. 4 (2018) 400–406.
[68] L.A.A. Bunthof, S. Veelenturf, E.J. Haverkamp, W.H.M. Corbeek, D. van der Woude, G.J. Bauhuis, P. Mulder, E. Vlieg, J.J. Schermer, Partially shaded III-V concentrator solar cell performance, Solar Energy Mater. Solar Cells 179 (2018) 231–240.
[69] S. Pareek, R. Dahiya, Enhanced power generation of partial shaded photovoltaic fields by forecasting the interconnection of modules, Energy 95 (2016) 561–572.
[70] M.N. Bhukya, V.R. Kota, A quick and effective MPPT scheme for solar power generation during dynamic weather and partial shaded conditions, Eng. Sci. Technol. Int. J. 22 (3) (2019) 869–884.

[71] E. Kandemir, N.S. Cetin, S. Borekci, A comprehensive overview of maximum power extraction methods for PV systems, Renew. Sustain. Energy Rev. 78 (2017) 93–112.
[72] K. Chandrasekaran, S. Sankar, K. Banumalar, Partial shading detection for PV arrays in a maximum power tracking system using the sine-cosine algorithm, Energy Sustain. Dev. 55 (2020) 105–121.
[73] M.B. Ogaard, H.N. Riise, H. Haug, S. Sartori, J.H. Selj, Photovoltaic system monitoring for high latitude locations, Solar Energy 207 (2020) 1045–1054.
[74] E. Piccoli, A. Dama, A. Dolara, S. Leva, Experimental validation of a model for PV systems under partial shading for building integrated applications, Solar Energy 183 (2019) 356–370.
[75] D. Wang, T. Qi, Y. Liu, Y. Wang, J. Fan, Y. Wang, H. Du, A method for evaluating both shading and power generation effects of rooftop solar PV panels for different climate zones of China, Solar Energy 205 (2020) 432–445.
[76] A. Wang, Y. Xuan, Multiscale prediction of localized hot-spot phenomena in solar cells, Renewable Energy 146 (2020) 1292–1300.
[77] N. Agrawal, B. Bora, A. Kapoor, Experimental investigations of fault tolerance due to shading in photovoltaic modules with different interconnected solar cell networks, Solar Energy 211 (2020) 1239–1254.
[78] E. Diaz-Dorado, J. Cidras, C. Carrillo, Discrete I-V model for partially shaded PV-arrays, Solar Energy 103 (2014) 96–107.
[79] P. Rajput, M. Malvoni, N.M. Kumar, O.S. Sastry, G.N. Tiwari, Risk priority number for understanding the severity of photovoltaic failure modes and their impacts on performance degradation, Case Stud. Therm. Eng. 16 (2019), 100563.
[80] G. Li, Y. Jin, M.W. Akram, X. Chen, J. Ji, Application of bio-inspired algorithms in maximum power point tracking for PV systems under partial shading conditions – A review, Renew. Sustain. Energy Rev. 81 (1) (2018) 840–873.
[81] R. Kumar, S. Khandelwal, P. Upadhyay, S. Pulipaka, Global maximum power point tracking using variable time and p-v curve region shifting technique along with incremental conductance for partially shaded photovoltaic systems, Solar Energy 189 (2019) 151–178.
[82] C. Han, H. Lee, Investigation and modeling of long-term mismatch loss of photovoltaic array, Renewable Energy 121 (2018) 521–527.
[83] M.C. Lopez-Escalante, F.M. Jiménez, M.G. Pérez, D. Leinen, J.R.R. Barrado, Shunt resistance criterion: design and implementation for industrial silicon solar cell production, Solar Energy 206 (2020) 269–278.
[84] M.H. Ali, A. Rabhi, A. El hajjaji, G.M. Tina, Real time fault detection in photovoltaic systems, Energy Procedia 111 (2017) 914–923.
[85] Y.-K. Wu, S.M. Chang, Y.-L. Hu, Literature review of power system blackouts, Energy Procedia 141 (2017) 428–431.
[86] S. Pareek, N. Chaturvedi, R. Dahiya, Optimal interconnections to address partial shading losses in solar photovoltaic arrays, Solar Energy 155 (2017) 537–551.
[87] A. Boccalatte, M. Fossa, R. Sacile, Modeling, design and construction of a zero-energy PV greenhouse for applications in mediterranean climates, Therm. Sci. Eng. Progress 25 (2021), 101046.
[88] A.S. Vaka, P. Talukdar, Novel inverse heat transfer technique for estimation of properties and location-specific process parameters of roof-mounted solar PV plants, Therm. Sci. Eng. Progress 19 (2020), 100657.
[89] S.R. Abdallah, I.M.M. Elsemary, A.A. Altohamy, M.A. Abdelrahman, A.A.A. Attia, O.E. Abdellatif, Experimental investigation on the effect of using nano fluid (Al2O3-Water) on the performance of PV/T system, Therm. Sci. Eng. Progress 7 (2018) 1–7.
[90] E. Johnston, P.S.B. Szabo, N.S. Bennett, Cooling silicon photovoltaic cells using finned heat sinks and the effect of inclination angle, Therm. Sci. Eng. Progress 23 (2021), 100902.
[91] A.N. Shmroukh, Thermal regulation of photovoltaic panel installed in Upper Egyptian conditions in Qena, Therm. Sci. Eng. Progress 14 (2019), 100438.
[92] S.R.M. Baygi, S.M. Sadrameli, Thermal management of photovoltaic solar cells using polyethylene glycol 1000 (PEG1000) as a phase change material, Therm. Sci. Eng. Progress 5 (2018) 405–411.
[93] A.H.A. Al-Waeli, H.A. Kazem, M.T. Chaichan, K. Sopian, Experimental investigation of using nano-PCM/nanofluid on a photovoltaic thermal system (PVT): technical and economic study, Therm. Sci. Eng. Progress 11 (2019) 213–230.
[94] S.R. Pendem, S. Mikkili, Modelling and performance assessment of PV array topologies under partial shading conditions to mitigate the mismatching power losses, Solar Energy 160 (2018) 303–321.
[95] T. Ramesh, K. Rajani, A.K. Panda, A novel triple-tied-cross-linked PV array configuration with reduced number of cross-ties to extract maximum power under partial shading conditions, CSEE J. Power Energy Syst. 7 (3) (2020) 567–581.
[96] F. Bayrak, H.K. Oztop, Effects of static and dynamic shading on thermodynamic and electrical performance for photovoltaic panels, Appl. Therm. Eng. 169 (2020), 114900.
[97] G. Shankar, V. Mukherjee, MPP detection of a partially shaded PV array by continuous GA and hybrid PSO, Ain Shams Eng. J. 6 (2) (2015) 471–479.
[98] J. Ma, X. Pan, K.L. Man, X. Li, H. Wen, T.O. Ting, Detection and assessment of partial shading scenarios on photovoltaic strings, IEEE Trans. Ind. Appl. IEEE 54 (6) (2018) 6279–6289.
[99] J.R. Louis, S. Shanmugham, K. Gunasekar, N.R. Atla, K. Murugesan, Effective utilisation and efficient maximum power extraction in partially shaded photovoltaic systems using minimum-distance-average-based clustering algorithm, IET Renewable Power Generation 10 (3) (2016) 319–326.
[100] A.A. Desai, S. Mikkili, Modelling and analysis of PV configurations (alternate TCT-BL, total cross tied, series, series parallel, bridge linked and honey comb) to extract maximum power under partial shading conditions, CSEE J. Power Energy Syst. (2020) 1–16.
[101] K. Lappalainen, S. Valkealahti, Effects of irradiance transition characteristics on the mismatch losses of different electrical PV array configurations, IET Renewable Power Generation 11 (2) (2017) 248–254.
[102] K. Osmani, A. Haddad, T. Lemenand, B. Castanier, M. Ramadan, Material based fault detection methods for PV systems, Key Eng. Mater. 856 (2020) 111–115.
[103] J.L. Prol, Regulation, profitability and diffusion of photovoltaic grid-connected systems: a comparative analysis of Germany and Spain, Renew. Sustain. Energy Rev. 91 (2018) 1170–1181.
[104] B. Steffen, Estimating the cost of capital for renewable energy projects, Energy Econ. 88 (2020), 104783.
[105] Md.S. Chowdhury, K.S. Rahman, T. Chowdhury, N. Nuthammachot, K. Techato, Md Akhtaruzzaman, S.K. Tiong, K. Sopian, N. Amin, An overview of solar photovoltaic panels' end-of-life material recycling, Energy Strategy Rev. 27 (2020), 100431.
[106] F.H. Alharbi, S. Kais, Theoretical limits of photovoltaics efficiency and possible improvements by intuitive approaches learned from photosynthesis and quantum coherence, Renew. Sustain. Energy Rev. 43 (2015) 1073–1089.
[107] A. Elamim, B. Hartiti, A. Haibaoui, A. Lfakir, P. Thevenin, Performance evaluation and economical analysis of three photovoltaic systems installed in an institutional building in Errachidia, Morocco, Energy Procedia 147 (2018) 121–129.
[108] T. AlSkaif, S. Dev, L. Visser, M. Hossari, W. van Sark, A systematic analysis of meteorological variables for PV output power estimation, Renewable Energy. 153 (2020) 12–22.
[109] V. Matulaitis, G. Straukaite, B. Azzopardi, E.A. Martinez-Cesena, Multi-criteria decision making for PV deployment on a multinational level, Solar Energy Mater. Solar Cells 156 (2016) 122–127.
[110] M. Balato, L. Costanzo, M. Vitelli, Reconfiguration of PV modules: a tool to get the best compromise between maximization of the extracted power and minimization of localized heating phenomena, Solar Energy 138 (2016) 105–118.
[111] R.K. Pachauri, O.P. Mahela, A. Sharma, J. Bai, Y.K. Chauhan, B. Khan, H. H. Alhelou, Impact of partial shading on various PV array configurations and different modeling approaches: a comprehensive review, IEEE Access 8 (2020) 181375–181403.
[112] S.G. Krishna, T. Moger. 2020. Static Reconfiguration approach for Photovoltaic Array to Improve Maximum power. 2020 International Conference on Electrical and Electronics Engineering (ICE3). IEEE. ISBN: 978-1-7281-5847-1.
[113] Y. Hu, J. Zhang, P. Li, D. Yu, L. Jiang, Non-uniform aged modules reconfiguration for large-scale PV array, IEEE Trans. Device Mater. Reliab. 17 (3) (2017) 560–569.
[114] G.S. Krishna, T. Moger. 2018. SuDoKu and Optimal SuDoKu Reconfiguration for TCT PV array Under Non-Uniform Irradiance Condition. 2018 IEEE 8th Power India International Conference (PIICON). IEEE. ISBN: 978-1-5386-7339-3.
[115] B.I. Rani, G.S. Ilango, C. Nagamani, Enhanced power generation from PV array under partial shading conditions by shade dispersion using Su Do Ku configuration, IEEE Trans. Sustain. Energy 4 (3) (2013) 594–601.
[116] N.D. Tuyen, L.V. Thinh, V.X.S. Huu. 2020. On the Sudoku-based Arrangement in Reconfiguring a Large-scale Photovoltaic Array. 2020 59th Annual Conference of the Society of Instrument and Control Engineers of Japan (SICE). IEEE. ISBN: 978-1-7281-1089-9.
[117] N.A. Rajan, K.D. Shrikant, B. Dhanalakshmi, N. Rajasekar, Solar PV array reconfiguration using the concept of Standard deviation and Genetic algorithm, Energy Procedia 117 (2017) 1062–1069.
[118] G.S. Krishna, T. Moger, Reconfiguration strategies for reducing partial shading effects in photovoltaic arrays: state of the art, Solar Energy 182 (2019) 429–452.
[119] S.G. Krishna, T. Moger, Optimal SuDoKu reconfiguration technique for total-cross-tied PV array to increase power output under non-uniform irradiance, IEEE Trans. Energy Convers. 34 (4) (2019) 1973–1984.
[120] G.S. Krishna, T. Moger, Improved SuDoKu reconfiguration technique for total-cross-tied PV array to enhance maximum power under partial shading conditions, Renew. Sustain. Energy Rev. 109 (2019) 333–348.
[121] S.V. Lokanath, B. Skarbek, E.J. Schindelholz. 2019. Chapter 9 – Degradation Processes and Mechanisms of PV Wires and Connectors. Durability and Reliability of Polymers and Other Materials in Photovoltaic Modules, Plastics Design Library. William Andrew. pp. 217-33.
[122] S.R. Potnuru, D. Pattabiraman, S.I. Ganesan, N. Chilakapati, Positioning of PV panels for reduction in line losses and mismatch losses in PV array, Renewable Energy 78 (2015) 264–275.
[123] B. Dhanalakshmi, N. Rajasekar, A novel Competence Square based PV array reconfiguration technique for solar PV maximum power extraction, Energy Convers. Manage. 174 (2018) 897–912.
[124] M.S.S. Nihanth, J.P. Ram, D.S. Pillai, A.M.Y.M. Ghias, A. Garg, N. Rajasekar, Enhanced power production in PV arrays using a new skyscraper puzzle based one-time reconfiguration procedure under partial shade conditions (PSCs), Solar Energy 194 (2019) 209–224.
[125] L. El Iysaouy, M. Lahbabi, A. Oumnad, A novel magic square view topology of a PV system under partial shading condition, Energy Procedia 157 (2019) 1182–1190.
[126] A.S. Yadav, R.K. Pachauri, Y.K. Chauhan, S. Choudhury, R. Singh, Performance enhancement of partially shaded PV array using novel shade dispersion effect on magic-square puzzle configuration, Solar Energy 144 (2017) 780–797.
[127] S.S. Reddy, C. Yammani, A Novel Magic-Square puzzle based one-time PV reconfiguration technique to mitigate mismatch power loss under various partial shading conditions, Optik 222 (2020), 165289.

[128] B. Dhanalakshmi, N. Rajasekar, Dominance square based array reconfiguration scheme for power loss reduction in solar PhotoVoltaic (PV) systems, Energy Convers. Manage. 156 (2018) 84–102.

[129] H.S. Sahu, S.K. Nayak, S. Mishra, Maximizing the power generation of a partially shaded PV array, IEEE J. Emerg. Selected Top. Power Electron. 4 (2) (2015) 626–637.

[130] H.S. Sahu, S.K. Nayak. 2014. Power enhancement of partially shaded PV array by using a novel approach for shade dispersion. 2014 IEEE Innovative Smart Grid Technologies – Asia (ISGT ASIA). IEEE. ISBN: 978-1-4799-1300-8.

[131] A.S. Yadav, V. Mukherjee, Lines losses reduction techniques in puzzled PV array configuration under different shading conditions, Solar Energy 171 (2018) 774–783.

[132] S.G. Krishna, T. Moger. 2020. A Novel Fixed Interconnection Topology for Photovoltaic Array to Gain Maximum Energy Yields. 2020 International Conference on Electrical and Electronics Engineering (ICE3). IEEE. ISBN: 978-1-7281-5846-4.

[133] S. Anjum, V. Mukherjee, G. Mehta, Modelling and simulation of AdDoKu based reconfiguration technique to harvest maximum power from photovoltaic array under partial shading conditions, Simul. Model. Pract. Theory 115 (2022), 102447.

[134] R.K. Pachauri, S.B. Thanikanti, J. Bai, V.K. Yadav, B. Aljafari, S. Gosh, H. H. Alhelou, Ancient Chinese magic square-based PV array reconfiguration methodology to reduce power loss under partial shading conditions, Energy Convers. Manage. 253 (2022), 115148.

[135] S. Anjum, V. Mukherjee, A novel arithmetic sequence pattern reconfiguration technique for line loss reduction of photovoltaic array under non-uniform irradiance, J. Clean. Prod. 331 (2022), 129822.

[136] I. Nasiruddin, S. Khatoon, M.F. Jalil, R.C. Bansal, Shade diffusion of partial shaded PV array by using odd-even structure, Solar Energy 181 (2019) 519–529.

[137] S.S. Reddy, C. Yammani, Odd-Even-Prime pattern for PV array to increase power output under partial shading conditions, Energy 213 (2020), 118780.

[138] D.S. Pillai, N. Rajasekar, J.P. Ram, V.K. Chinnaiyan, Design and testing of two phase array reconfiguration procedure for maximizing power in solar PV systems under partial shade conditions (PSC), Energy Convers. Manage. 178 (2018) 92–110.

[139] R. Venkateswari, N. Rajasekar, Power enhancement of PV system via physical array reconfiguration based Lo Shu technique, Energy Convers. Manage. 215 (2020), 112885.

[140] A.S. Yadav, R.K. Pachauri, Y.K. Chauhan, Comprehensive investigation of PV arrays with puzzle shade dispersion for improved performance, Solar Energy 129 (2016) 256–285.

[141] Z. Yang, N. Zhang, J. Wang, Y. Liu, L. Fu, Improved non-symmetrical puzzle reconfiguration scheme for power loss reduction in photovoltaic systems under partial shading conditions, Sustain. Energy Technol. Assess. 51 (2022), 101934.

[142] S. Vijayalekshmy, G.R. Bindu, S.R. Iyer, A novel Zig-Zag scheme for power enhancement of partially shaded solar arrays, Solar Energy 135 (2016) 92–102.

[143] N. Belhaouas, M.-S.-A. Cheikh, P. Agathoklis, M.-R. Oularbi, B. Amrouche, K. Sedraoui, N. Djilali, PV array power output maximization under partial shading using new shifted PV array arrangements, Appl. Energy 187 (2017) 326–337.

[144] P.R. Satpathy, R. Sharma, S. Dash, An efficient SD-PAR technique for maximum power generation from modules of partially shaded PV arrays, Energy 175 (2019) 182–194.

[145] P.R. Satpathy, R. Sharma, Power loss reduction in partially shaded PV arrays by a static SDP technique, Energy 156 (2018) 569–585.

[146] J. Storey, P.R. Wilson, D. Bagnall, The optimized-string dynamic photovoltaic array, IEEE Trans. Power Electron. 29 (4) (2013) 1768–1776.

[147] M. Balato, L. Costanzo, M. Vitelli, Series-Parallel PV array re-configuration: maximization of the extraction of energy and much more, Appl. Energy 159 (2015) 145–160.

[148] O. Bingol, B. Ozkaya, Analysis and comparison of different PV array configurations under partial shading conditions, Solar Energy 160 (2018) 336–343.

[149] D. Picault, B. Raison, S. Bacha, J. de la Casa, J. Aguilera, Forecasting photovoltaic array power production subject to mismatch losses, Solar Energy 84 (7) (2010) 1301–1309.

[150] S. Mohammadnejad, A. Khalafi, S.M. Ahmadi, Mathematical analysis of total-cross-tied photovoltaic array under partial shading condition and its comparison with other configurations, Solar Energy 133 (2016) 501–511.

[151] M.Z. Shams El-Dein, M. Kazerani, M.M.A. Salama, Optimal photovoltaic array reconfiguration to reduce partial shading losses, IEEE Trans. Sustain. Energy 4 (1) (2013) 145–153.

[152] T.S. Babu, D. Yousri, K. Balasubramanian, Photovoltaic array reconfiguration system for maximizing the harvested power using population-based algorithms, IEEE Access 8 (2020) 109608–109624.

[153] A. Fathy, Recent meta-heuristic grasshopper optimization algorithm for optimal reconfiguration of partially shaded PV array, Solar Energy 171 (2018) 638–651.

[154] A. Fathy, Butterfly optimization algorithm based methodology for enhancing the shaded photovoltaic array extracted power via reconfiguration process, Energy Convers. Manage. 220 (2020), 113115.

[155] E.R. Sanseverino, T.N. Ngoc, M. Cardinale, V.L. Vigni, D. Musso, P. Romano, F. Viola, Dynamic programming and Munkres algorithm for optimal photovoltaic arrays reconfiguration, Solar Energy 122 (2015) 347–358.

[156] H. Tian, F. Mancilla-David, K. Ellis, E. Muljadi, P. Jenkins, Determination of the optimal configuration for a photovoltaic array depending on the shading condition, Solar Energy 95 (2013) 1–12.

[157] M. Alahmad, M.A. Chaaban, S.K. Lau, J. Shi, J. Neal, An adaptive utility interactive photovoltaic system based on a flexible switch matrix to optimize performance in real-time, Solar Energy 86 (3) (2012) 951–963.

[158] L.F.L. Villa, T.-P. Ho, J.-C. Crebier, B. Raison, A power electronics equalizer application for partially shaded photovoltaic modules, IEEE Trans. Ind. Electron. 60 (3) (2012) 1179–1190.

[159] P.S. Rao, G.S. Ilango, C. Nagamani, Maximum power from PV arrays using a fixed configuration under different shading conditions, IEEE J. Photovoltaics 4 (2) (2014) 679–686.

[160] A.A. Heidari, S. Mirjalili, H. Faris, I. Aljarah, M. Mafarja, H. Chen, Harris hawks optimization: algorithm and applications, Fut. Gener. Comput. Syst. 97 (2019) 849–872.

[161] D. Yousri, D. Allam, M.B. Eteiba, Optimal photovoltaic array reconfiguration for alleviating the partial shading influence based on a modified harris hawks optimizer, Energy Convers. Manage. 206 (2020), 112470.

[162] V.K. Yadav, A. Yadav, R. Yadav, A. Mittal, N.H. Wazir, S. Gupta, R.K. Pachauri, S. Ghosh, A novel reconfiguration technique for improvement of PV reliability, Renewable Energy 182 (2022) 508–520.

[163] P. dos Santos, E.M. Vicente, E.R. Ribeiro. 2011. Reconfiguration methodology of shaded photovoltaic panels to maximize the produced energy. XI Brazilian Power Electronics Conference. IEEE. ISBN: 978-1-4577-1646-1.

[164] Z. Cheng, Z. Pang, Y. Liu, P. Xue. 2010. An adaptive solar photovoltaic array reconfiguration method based on fuzzy control. 2010 8th World Congress on Intelligent Control and Automation. IEEE. ISBN: 978-1-4244-6712-9.

[165] H. Ziar, E. Afjei, A. Siadatan, A. Arjhangmehr. 2011. Different diode configurations evaluation in photovoltaic arrays using binary coding method. International Aegean Conference on Electrical Machines and Power Electronics and Electromotion, Joint Conference. IEEE. ISBN: 978-1-4673-5003-7.

[166] R. Cavieres, R. Barraza, D. Estay, J. Bilbao, P. Valdivia-Lefort, Automatic soiling and partial shading assessment on PV modules through RGB images analysis, Appl. Energy 306 (2022), 117964.

[167] M. Waqar Akram, G. Li, Y. Jin, X. Chen, C. Zhu, X. Zhao, M. Aleem, A. Ahmad, Improved outdoor thermography and processing of infrared images for defect detection in PV modules, Solar Energy 190 (2019) 549–560.

[168] L. Pratt, D. Govender, R. Klein, Defect detection and quantification in electroluminescence images of solar PV modules using U-net semantic segmentation, Renewable Energy 178 (2021) 1211–1222.

[169] A.M. Moradi Sizkouhi, S.M. Esmailifar, M. Aghaei, M. Karimkhani, RoboPV: an integrated software package for autonomous aerial monitoring of large scale PV plants, Energy Convers. Manage. 254 (2022), 115217.

[170] M. Karakose, M. Baygin. 2014. Image processing based analysis of moving shadow effect for reconfiguration in PV arrays. 2014 IEEE International Energy Conference (ENERGYCON). IEEE. ISBN: 978-1-4799-2449-3.

[171] M. Etarhouni, B. Chong, L. Zhang, A combined scheme for maximising the output power of a Photovoltaic array under partial shading conditions, Sustain. Energy Technol. Assess. 50 (2022), 101878.

[172] G.M. Masters, Chapter 5 – Photovoltaic materials and electrical characteristics, in: Renewable and Efficient Electric Power Systems, 2nd Edition., Wiley-IEEE Press, 2013, pp. 253–301.

[173] G.M. Masters, Chapter 6 – Photovoltaic systems, in: Renewable and Efficient Electric Power Systems, 2nd Edition., Wiley-IEEE Press, 2013, pp. 316–387.

[174] V.B. Raju, C.h. Chengaiah, A comprehensive study on re-arrangement of modules based TCT configurations of partial shaded PV array with shade dispersion method, Trends Renew. Energy 6 (2020) 37–60.

[175] M. Premkumar, U. Subramaniam, T.S. Babu, R.M. Elavarasan, L. Mihet-Popa, Evaluation of mathematical model to characterize the performance of conventional and hybrid PV array topologies under static and dynamic shading patterns, Energies 13 (12) (2020) 24–37.

[176] A.M. Ajmal, V.K. Ramachandaramurthy, A. Naderipour, J.B. Ekanayake, Comparative analysis of two-step GA-based PV array reconfiguration technique and other reconfiguration techniques, Energy Convers. Manage. 230 (2021), 113806.